Universidade de Aveiro
Ano 2018

Departamento de Eletrónica Telecomunicações e Informática

Miguel Pais Machado

Visible Light Communications for Drivers Assistance Systems

Sistemas de Comunicação por Luz Visível Aplicados para Assistência ao Tráfego Automóvel

Universidade de Aveiro
Ano 2018

Departamento de Eletrónica Telecomunicações e Informática

Miguel Pais Machado

Visible Light Communications for Drivers Assistance Systems

Sistemas de Comunicação por Luz Visível Aplicados para Assistência ao Tráfego Automóvel

Dissertação apresentada à Universidade de Aveiro para cumprimento dos requisitos necessários à obtenção do grau de Mestre em Engenharia Eletrónica e Telecomunicações, realizada sob a orientação científica do Doutor Luis Nero Alves, Professor Auxiliar do Departamento de Eletrónica, Telecomunicações e Informática da Universidade de Aveiro

Dedico este trabalho a todos os que me empurraram para a frente.

o júri

Presidente	**Prof. Doutora Susana Isabel Barreto de Miranda Sargento** Professora Associada C/ Agregação do Departamento de Engenharia Eletrónica, Telecomunicações e Informática da Universidade de Aveiro
Orientador	**Prof. Doutor Luis Filipe Mesquita Nero Moreira Alves** Professor Auxiliar do Departamento de Engenharia Eletrónica, Telecomunicações e Informática da Universidade de Aveiro
Arguente	**Prof. Doutora Mónica Jorge Carvalho Figueiredo** Professora Adjunta do Departamento de Engenharia Eletrotécnica da Escola Superior de Tecnologia e Gestão do Instituto Politécnico de Leiria

Acknowledgements

The proposed topic was a chance to develop new knowledge about optical wireless communications, contribute to an ongoing project as well as to synthetize and review innumerable aspects and subjects lectured along the master's course. This dissertation covers my final work as a student of University of Aveiro, and more singularly marks the end to an era of studies on the master's course on Electronical and Telecommunications Engineering.

It is now time for a new adventure outside the academic world, but I shall cherish everyone that have helped me along this path. Without disregard to anyone that I may forget to mention, here goes the owed thanks in the development of this work:

To my supervisor Professor Luis Filipe Mesquita Nero Moreira Alves, for the continuous support and belief.

To all my colleagues in the laboratory for integrated circuits, Luis Abade, Luis Rodrigues, Debarati, Shusmitha, João, André, Patricia, Miguel and other's that contribute to the group, for a great work environment, for being a good source of information and discussion.

To the Telecommunications institute of Aveiro (IT), for providing the facilities and resources.

To all the teachers along the way, old and new.

To my parents, Maria Isabel da Costa Pais and José Carlos Soares Machado e Silva, for all the love and patience they had with me and to all friends who had the ability of understanding the difficult plight the last year has been.

palavras-chave I2C, C2C, linha de visão, radiação difusa, relação sinal-ruido, taxa de erro, fontes de ruido

resumo

Motivado em promover o tópico de segurança rodoviária e sistemas de informação, este trabalho providência um estudo dedicado a sistemas de comunicação por luz visível (VLC) para aplicação em cenários de exterior. O tópico desenvolvido faz parte de sistemas de transporte inteligentes (ITS) cujo propósito é a disseminação de sistemas de segurança no tráfego e transferência de informação, para aplicações de segurança. A tecnologia VLC aplicada a sistemas de comunicação de tráfego rodoviário suscita elevado interesse devido a vantagens que esta apresenta. O uso de LED's em semáforos e faróis de carros começa a ser bastante comum. Com a combinação de diferentes valências, como iluminação e transferência de dados no mesmo dispositivo, a tecnologia VLC torna-se muito atrativa para a implementação em sistema de comunicação exterior dedicados a sistemas de informação e controlo de tráfego.

O canal de comunicação VLC exterior apresenta condições variáveis, devido ao fato de existirem condições ambientais diferentes. Um grave problema neste tipo de canal de comunicação é a presença de ruido Shot, que é normalmente gerado devido á radiância causada por diferentes fontes de luz de fundo.

Nesta dissertação estão presentes dois tipos de cenários para sistemas de informação de tráfego, em que o primeiro dedica-se á comunicação semáforo-carro (I2C) e o segundo cenário para a comunicação entre carros (C2C). Para simular o desempenho do canal de comunicação com diferentes condições ambientais, foram implementados em MATLAB modelos para a propagação ótica, descrição do emissor, recetor e fontes de ruido. Também foram incluídos modelos para diferentes fontes óticas de radiação, com medições de campo da iluminância incidente num foto recetor e modulado o impacto na geração de ruido.

Nas simulações de desempenho da comunicação por luz visível, foram considerados diferentes esquemas de modulação da informação com o intuito de avaliar o desempenho da ligação, a qual foi feita recorrendo a métricas clássicas de desempenho de modulações digitais.

keywords I2C, C2C, line-of-sight, diffuse radiation, signal-to-noise, bit-error-rate, optical noise

abstract Motivated by the topic of promoting traffic safety applications and information systems, this work aims to bring a study on VLC outdoor application scenarios. The developed topic is part of intelligent transportation systems (ITS) that aim at the delivery of traffic safety and information amongst other safety functions. VLC technology in traffic communication applications gains interest due to some advantages it presents. The use of LEDs in traffic signaling infrastructures and vehicle headlights started to be a growing standard. With the combination of illuminating proprieties and communication in the same device, VLC becomes a very attractive technology for the implementation of outdoor communication systems for traffic information and control.

Outdoor VLC channels present variable ambient conditions, with the presence of different optical sources. One major problem in this communication channel is the presence of shot-noise, generated by optical background radiance from different light sources.

This dissertation presents two different communication scenarios for traffic information systems, the first being directed at the infrastructure to car (I2C) link and the second one for car to car (C2C) communication. In order to simulate the communication link performance with variable ambient channel conditions, several models for optical propagation, emitter, receiver and noise sources were implemented in MATLAB. Models for different optical sources were also implemented, with field measurements on the illuminance incident on a photo detector and their impact on the noise generated.

In the simulation's performance of the VLC link, several baseband modulation schemes were considered, aiming at the assessment of link performance, based on the traditional digital modulation performance metrics.

Contents

List of Figures

List of Tables

Acronyms

AM	Amplitude modulation
AWGN	Additive white gaussian noise
APD	Avalanche photodetector
BER	Bit error rate
C2C	Car to car
CIR	Channel impulse response
DD	Direct detection
DH-PIM	Dual header pulse interval modulation
DPIM	Differential pulse interval modulation
DRMS	Delay root mean square
EM	Electromagnetic
FM	Frequency modulation
FOV	Field of view
I2C	Infrastructure to car
IM	Impulse modulation
IR	infrared
ISI	Inter symbol interference
LAN	Local area network
LD	Laser diode
LED	Light emitting diode
LOS	Line of sight
ODAC	Optical digital to analogue converter
OOK	On off keying

OWC	Optical wireless communications
PAPR	Peak to average power ratio
PD	Photodetector
PER	Packet error rate
PM	Phase modulation
PSD	Power spectral distribution
PPM	Pulse position modulation
RF	Radio frequency
SER	Symbol error rate
SNR	Signal to noise ratio
Sr	Steradian
VLC	Visible light communication

1. Chapter 1

1.1 Introduction

In today's world the voracity for information and entertainment is straining the available user bandwidth regarding the individual consume, where common people dry out the available RF spectrum [1] in telecommunications networks causing blockage and poor access to services, especially in crowded events. In VLC (visible light communication) the available spectrum is between 430 THz and 770 THz, as showed in fig. 1.1 [2] which comprises a very wide slice of the electromagnetic spectrum, offering freedom in terms of spectrum regulation and bandwidth availability.

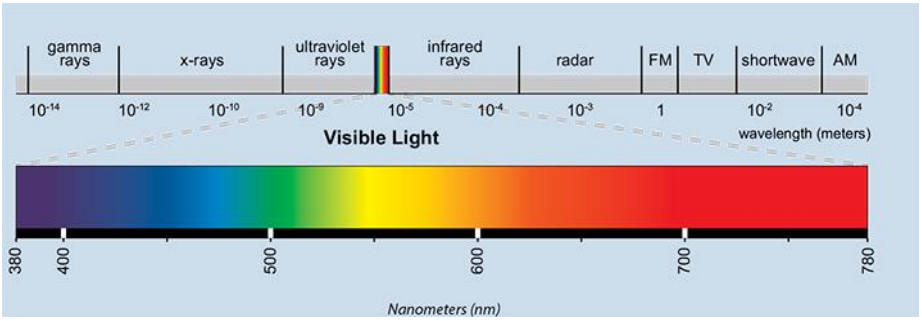

Figure 1.1 Electromagnetic Spectrum [2]

The use of optical sources to convey information was always embedded in human nature. Ancient tribes used bonfires to signal an event that could be spotted from afar, it was especially useful when scouts wanted to inform faster their side of an oncoming enemy army or raiding party. In the XVIII century a French inventor and scientist Claude Chappe, invented the optical telegraph [3], a system of towers spread throughout France, these towers had two arms on each side and a cross-arm connecting each other, as seen in figure 1.1, enabling a large number of discrete and different positions of the structure, so encoded messages could be relayed from tower to tower. Napoleon used this system to transmit and receive information through his empire. There is even the Graham Bell photo phone [4], from 1880, capable of wireless voice telephone message by

modulating a beam of light, it was capable of reaching a distance up to 213 meters. These were the ancestors of VLC in which they represent a natural human pursuit in the development of such technologies.

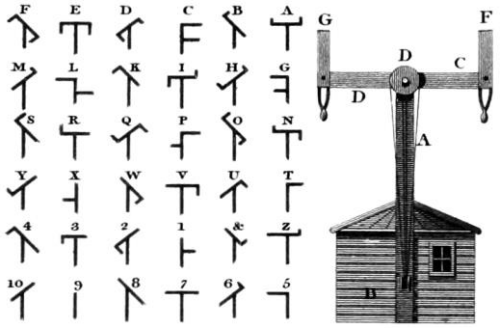

Figure 1.2 Claudde's Chappe optical telegraph [3]

VLC has been gaining interest of researchers and companies in the last two decades. It is only until recently that we have a disseminated resource that can modulate light to achieve meaningful data rates. This was due to continuous investment and development in the evolution of LED (light emitting diode) technology. Where it can be point out some factors such as the increase in the electrical-optical efficiency, a fairly linear relationship in terms of optical power vs current and also the high flickering capabilities in impulse modulation (IM) of the transmitted optical power in this kind of semiconductor enables the use of VLC systems. So it can be said that LEDs can be perceived as a high speed wireless transmitter, as so it is bandwidth can achieve values in the range of tenths MHz [5].

This work aims to use VLC in ITS (intelligent transportation systems) applications. ITS is a new trend trying to face arising problems in the growing road traffic. ITS is divided in three major architectures, finding different applications branches [6]:

- Infrastructure to car (I2C): intelligent traffic control, traffic information, traffic monitoring, emergency vehicle presence warning.
- Car to car (C2C): collision warning systems, cooperative traffic, situation awareness.
- Car to infrastructure (C2I): traffic management for priority vehicles, electronic tolling.

Currently the car and infrastructure lighting devices are being widely updated with LED technology, enabling VLC to play a major role in future ITS architectures.

1.2 Motivation

Since the beginning of the millennium, the percentage of fatalities related to car accidents that occur in city roads has increased in more than half of the IRTAD [7] (International Traffic Safety Data and Analysis Group) countries. In these group countries like Portugal, Greece and Korea present a significant increasing mortality associated to urban road traffic accidents. The Global status report [8] refers that the total number of road traffic deaths worldwide has reached the number of 1.25 million people in 2013. This statistic shows that there is a great necessity to decrease the human casualties related to this problem, ideally bringing them to zero. In order to be closer to this goal, many approaches have been considered, such as more restricted regulations on speed limits, seat belt use, policies to reduce drink-driving cases and better active restraint systems [8]. Intelligent transportation systems can be part of a solution designed to create a communication bridge between road entities in a traffic scenario, specifically cars and road associated infrastructure.

VLC can play a major role in ITS applications, providing several advantages over RF (radio frequency)[1]:

- Low complexity and cost: LEDs are already present in many possible application scenarios, such as car headlamps, signal traffic lights and street lights.
- High positioning: highly directional line of sight (LOS) propagation increases positioning accuracy.
- Improved link quality: high directional communication mitigates traffic congestion, particularly during rush hours.
- Security: offers higher security due to LOS propagation characteristics of VLC.
- Camera based communications: more complex receiver system, that allows spatially separation of different emitters.
- No spectrum regulation or licencing.

In VIDAS [9] one of the proposed scenarios for VLC, one of which is in scope in this work, was to develop a communication link between a traffic light signal and oncoming cars (I2C). One great remark of this project is to reutilize existing infrastructures such as the traffic light maintaining its original purpose and making it an emitter for visible light encoded data. The same can be said about the other scenario under scope C2C (car to car), the emitter would be implemented in the car's frontal beam lamps or the tailgate break lamps. Implementation of these communication links would provide necessary information to driver's for road traffic safety, the system would be able to

transmit traffic congestions in the nearby area, weather implications and accidents notices, and so on… This would be possible by integrating the visible light wireless information system with pre-existing traffic management systems like GERTRUDE [10] system in Lisbon. The possibilities for a C2C communication link can aid in the relay of information between cars of their relative positions, even automatically activate emergency brakes to avoid collision if the car ahead makes an unexpected stop. Even in a near future with the development of self-driving cars, C2C communication with OWC can provide an important tool in autonomous vehicles. So in a near future a LED lit car may not just be communicating with other nearby cars, but integrated in a complex mesh of devices in a city street grid [11].

1.2.1 VLC Applications

Everyday new ideas for applications in VLC are in development, where these are inherent to some specific positive proprieties in VLC which include decent bandwidth, light does not present any danger to the human body, low power consumption being a technology to be implemented in lightning devices, access security and no interference with electromagnetic sensitive equipment. Different applications for VLC which can include [12][13]:

- Hospitals – near electronically sensitive equipment like MRI scanner and operating theatres is undesirable to have Wi-Fi or mobile phones so it would be desirable to use VLC networks in these areas.
- Information displaying billboards – publicity sign and billboards often made from LED arrays where information can be modulated and received by a camera or other sensor in a user's smartphone. This type of marketing information augmentation could be used in various locations such as airports, museums, hospitals or any other kind of business.
- Wireless local area networks – a unique trait for VLC in data transmission, is that data cannot be accessed by any device not in the same room as the systems transceiver. Unlike radio-based systems, VLC systems are limited by physical barriers like walls, which visible light cannot pass through. This makes necessary for the user to be present and in the same room as the system, providing an additional security feature.
- Indoor localization – another possibility for VLC is an alternative to GPS, as this does not work properly inside buildings. Considering an arrangement of combination of

different lights as an emitter group it would be possible to locate receivers within a room using trilateration techniques. Applying receivers' tags to people and equipment would permit to discover their location.

1.3 Objectives

The main objectives in this work is to study and simulate the scenarios under scope (I2C, C2C), originally based on the VIDAS project [9], to better understand the necessities, impairments in this kind of wireless communication and trying to explore alternatives to the already developed VLC system in VIDAS. The constraints can be channel bandwidth, VLC's systems optical propagation, sources of optical noise interference and data encoding. In order to try to overcome or minimize the effects of limitations in VLC scenarios.

1.4 Dissertation structure

This dissertation includes the current chapter with the motivation, context and some VLC applications. In the next chapters there will be present the following topics by order:

- Study the emitter and receiver characteristics.
- Development of an I2C MATLAB scenario, for LOS optical propagation.
- Characterization of optical noise sources.
- System bandwidth limitations on the LED emitter.
- Proposed VLC modulation schemes analysis and performance comparison.
- Performance comparison of different modulation schemes with different optical noise ambient scenarios.
- Development of a C2C scenario with LOS and non-LOS diffuse link, with characterization of the channel.
- Multipath effects on the delay spread and channel bandwidth limitations.

2. Chapter 2

2.1 System Model Description

The purpose of designing a communication system is to deliver information from the emitter to the receiver without any difference from the source. There are many factors at play such as imperfections, receiver and emitter layout, channel noise and interference, signal attenuation or bad signal coverage, the received data is susceptible to error or even non-existent due to link loss.

To be able to design a VLC system is necessary to have in mind the full limitations and different elements in an optical wireless channel, to do this is required a mathematical model capable of describing the optical propagation as well as the emitter and receiver behaviour. In this chapter it is addressed channel modelling for VLC systems focused on the LOS link, which in an outdoor application severely restricts the data communication range. A typical I2C scenario is represented in fig. 2.1, where the signal traffic light (Tx) transmits an optical signal to the red car (Rx).

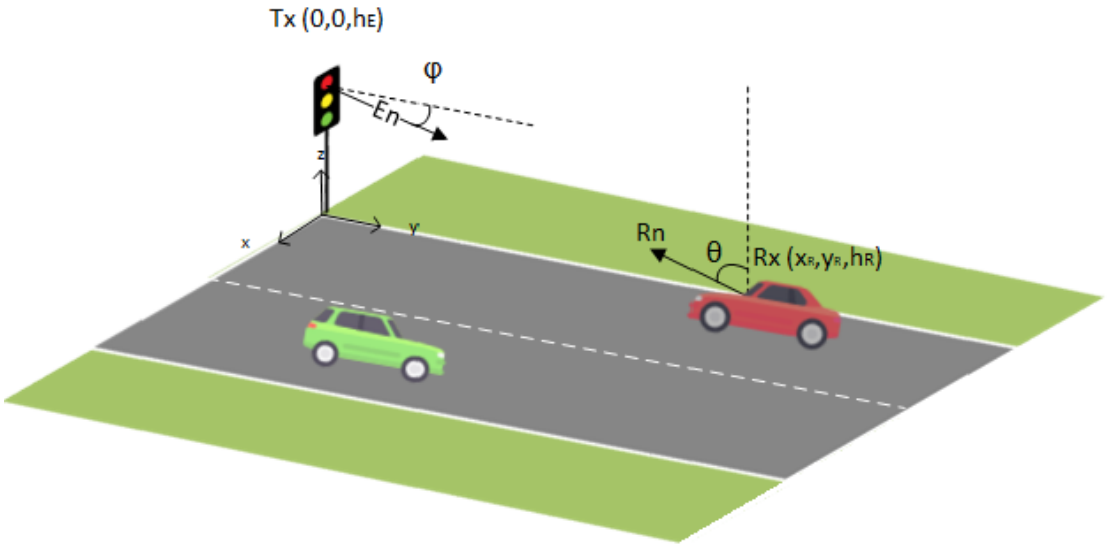

Figure 2.1 I2C scenario

To begin modelling the I2C scenario is necessary to analyse two basic characteristics of the LED emitter, the luminous intensity and the radiated optical power, these two metrics are directly correlated – being the first a measure of how a human being perceives the intensity of light and the second the energetic measure of the power radiated (photometric and radiometric relation explained further in this chapter). The emitter LED brightness and optical power will be conditioned

by proprieties of the LED itself and user safety regulations, therefore it also has a direct impact in the range of the data communication link in free space. Other major impairments arise with the presence of optical interference sources, some from natural origin (sunlight, moonlight), while others are artificial light (street lightning, other vehicles, etc.). The effect of this optical noise will have to be introduced in the receiver model, which normally is a photodetector diode [14][15][1].

2.2 Channel Modelling

The communication channel can be broken down into 3 distinct elements, the transmitter, the receiver and the physical space between them. The channel model revolves around the characterization of these three elements and their properties. Due to similarities of the communication medium between VLC and IR (infrared) systems, the knowledge gathered from extensive research in this predecessor's systems (IR) can be adapted to produce mathematical models for VLC [16].

2.2.1 Emitter technical characteristics

As discussed before the usage and development of LEDs has brought the necessary viability for high bandwidth VLC systems, their fast switching capabilities and electro-optical efficiency factors in this account. Upon researching several manufacturer's datasheet's for different type LEDs, it was identified the necessary type of technical parameters to define the emitter in the simulation scenarios.

Table 2-1 LED optical characteristics found on datasheet's

Manufacturer	**Model**	**Colour**	**Peak Wavelength**	**Optical Spectral Width**	**Luminous Intensity I_V[cd] @ I_F [mA]**	**Half power angle**
Vishay	TLCR5200	Red	616 nm	11 nm	4 cd @ 50mA	15°
	TLCY5200	yellow	593 nm	17 nm	4 cd @ 50mA	15°

	TLCTG5200	True Green	520 nm	37 nm	2 cd @ 30mA	15°
OSRAM	LR W5SM	Red	628 nm	18 nm	22 @ 400mA	60°
	LER Q8WP	Red	632 nm	18 nm	50 @ 1400mA	60°
Avago	HLMP-EG1A-Z10DD	Red	626 nm	28 nm	12-21 cd @ 20mA	15°
	HLMP-CM1G-350DD	Green	525 nm	20 nm	27-59 cd @ 20mA	15°
	HLMP-EL1A-Z1LDD	Amber	590 nm	13 nm	12-21 cd @20mA	15°

The light emitting diode is a semiconductor P-N junction, where under enough electrical potential applied to its terminals a current flows and electrical carriers (electrons) recombine with holes. In this recombination process is usually generated a photon, but sometimes non-radiative recombination can occur, and the energy is converted to vibrational energy (phonons) and thus the electric energy is converted to heat. The electro-optical efficiency (η) tends to decrease with increasing driving current, when high carrier injection occurs non-radiative recombination increases and vibrational heat is generated [17]. This deficiency in the LED electro-optical performance causes non-linear effects in the communication channel distorting the information sent, but for low injection current the behaviour is approximately linear. When evaluating the electro optical efficiency of a red LED [18], a linear approximation for the efficiency can be used as displayed in figure 2.2.

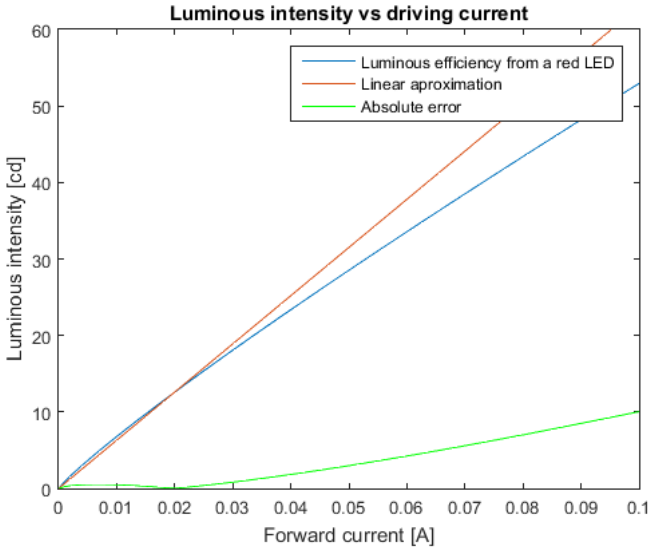

Figure 2.2 Electro optical LED efficiency

As it is displayed the luminous intensity (I_v) efficiency drops with the increase current through the LED. In the proposed interval it can be expect a relation between the optical intensity and forward current described by the electro-optical efficiency (η_v), relative to a single LED:

$$\frac{I_v}{I_{LED}} = \eta_v \left[\frac{\text{cd}}{\text{A}}\right] \quad (2.1)$$

The ratio between light output intensity from a single LED and the injection current, can also be modelled as [1]:

$$\eta_v = \frac{hv}{q} n_{int} n_{ex} \quad (2.2)$$

Where the electro optical efficiency depends on factors such as the internal quantum efficiency (n_{int}), which measures the effectiveness ratio of carrier photon generator to total number of carriers passing through the junction, the external efficiency (n_{ext}) represents the ratio of photons externally emitted by the device and not trapped or absorbed by imperfections in the LED casing, h is Planck constant, v the frequency of the generated photons and q the electron charge constant.

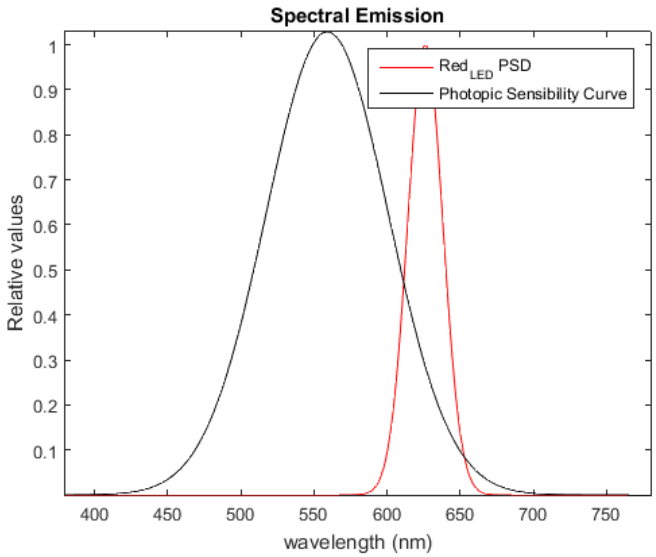

Figure 2.3 Normalized human eye spectral sensitivity curve and red LED spectral power

As it can be observed in fig. 2.3, LED as a light source is not monochromatic, the red LED spectral power distribution has its peak around 626 nm with optical spectral width around 28 nm. The relations established above in this subtopic are not wavelength dependent but based on photometric measures, like luminous intensity.

Photometry measures are analogous to radiometric units, as photometry is a branch of the wider field of radiometry. Radiometry can be considered as an independent entity capable of measuring the energy of electromagnetic radiation, while photometry considers the detector entity sensitivity to visible radiation, more specifically the sensitivity of the human visual system. Radiometry and photometry are also concerned with the optical power radiation for a given geometry of propagation. The photometric units analogous to the radiant flux ϕ_e, radiant intensity I_e, irradiance E_e and radiance L_e are the luminous flux ϕ_v, the luminous intensity I_v, the illuminance E_v and the luminance L_v [1].

Normally LED manufactures express their optical characteristics in photometric units, but the relation between the radiometry and photometry can be given by:

$$\phi_v = K_m \int_{380nm}^{780nm} \phi_e(\lambda).V(\lambda)d\lambda \qquad (2.3)$$

Where, V(λ) represents the normalized spectral sensitivity curve of the human visual system under daytime conditions, as seen in fig 2.3, the Km = 683 lm/W, is a constant establishing the radiometric to photometric sensitivity peak of the human physiological measure system. All the other photometric quantities are related to the weighted integral relationship of their corresponding radiometric units. To obtain the wavelength dependant optical power $\phi_e(\lambda)$, normally is used a powerful computing tool like MATLAB to invert the weighted sum interval on the visible slice of the spectrum.

2.2.2 Emitter Model

Normally LEDs optical power radiation is approximated by modelling the emitter as a single point source with a Lambertian radiation pattern, given by:

$$I(\phi) = I_0 . cos^m(\phi) \qquad (2.4)$$

The radiant intensity (W/sr) has its maximum when the viewing angle (ϕ) between the propagated light intensity and the emitter normal axis is 0 degrees and m is the mode number of the Lambertian emission that defines the directivity of the source. In figure 2.4, it shows a radiant intensity pattern for an ideal Lambertian source with m=1, equivalent to an LED with half power angle of 60° degrees.

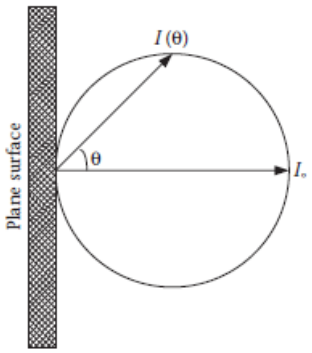

Figure 2.4 LED emission perpendicular to the junction plane[15]

$$m = \frac{-\ln 2}{\ln(\cos \phi_{1/2})} \quad (2.5)$$

Where $\phi_{1/2}$ is the half power angle of the LED dependent on geometric and encapsulation conditions of the semiconductor. The LED emitter is modelled using a generalized Lambertian radiation pattern [1], where the radiant intensity $R_E(\phi,m)$ is dependent on the viewing angle and the directivity of the source and assuming P_t as the total power emitted by it.

$$R_E(\phi, m) = \frac{m+1}{2\pi} P_t \cos^m(\phi); \quad \phi \in \left[-\frac{\pi}{2}; \frac{\pi}{2}\right] \quad (2.6)$$

The $\frac{m+1}{2\pi}$ coefficient ensures the integration of the radiant source power P_t over the directivity lobe of the emitter, to result in the radiant intensity emitted dependent on the emission angle as showed in equation 2.4. Which in this case of a Lambertian source of visible radiation establishes the relation between the radiant power and the radiant intensity of the LED.

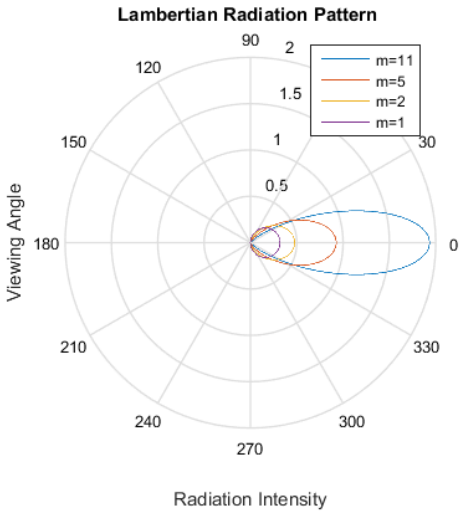

Figure 2.5 Polar plots of Lambertian radiation patterns

From equation 2.5, the directivity of the emitted power is dependant to the half power angle (*hpa*), the viewing angle at which 50% of the main emitted radiant intensity falls to its half value. Narrow *hpa* causes LEDs to have more axial directivity of the propagated power, but the radial intensity falls off more quickly. Figure 2.5, shows different radiant intensity patterns for different *hpa* values, corresponding to 20°, 30°, 45° and 60° degrees.

2.2.3 Traffic Light Emitter Matrix

LED signal traffic lights use high brightness LEDs connected in a combination of series and parallel to build a LED matrix, adding an optical lens is also necessary to have a uniform light distribution regarding the normal reference axis of the light emitter. In this subtopic is presented a circular LED arrangement and the resulting luminous intensity generated by the LED traffic light, considering the requirements in regulations for signal traffic lights.

The simulated LED matrix display (figure 2.6), has the following characteristics:

- 200 LEDs over 11 co-centric rings;
- Equal inner-ring LED spacing and equal inter-ring spacing;

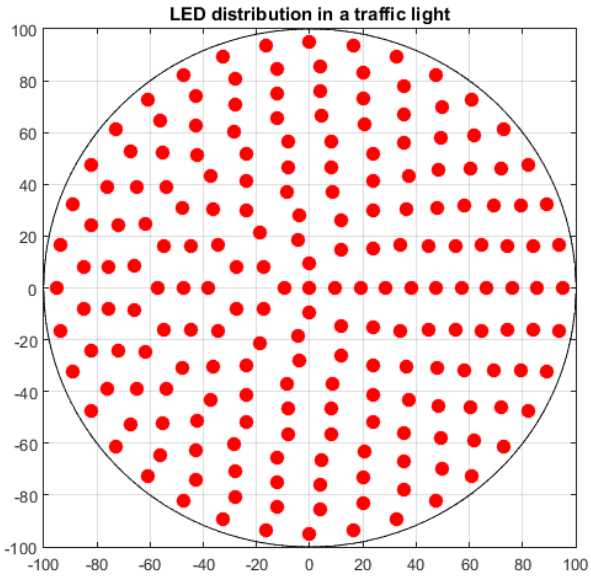

Figure 2.6 LED matrix (200mm)

The ring pattern of LEDs placed in co-centric circumferences, as shown in fig. 2.6, form a source of multiple LED Lambertian emitters. The models in this subchapter consider the emitting matrix as the centre of origin, in the Cartesian coordinate system (x,y,z), for simplification purposes the matrix emitting plane is parallel to the XoY plane.

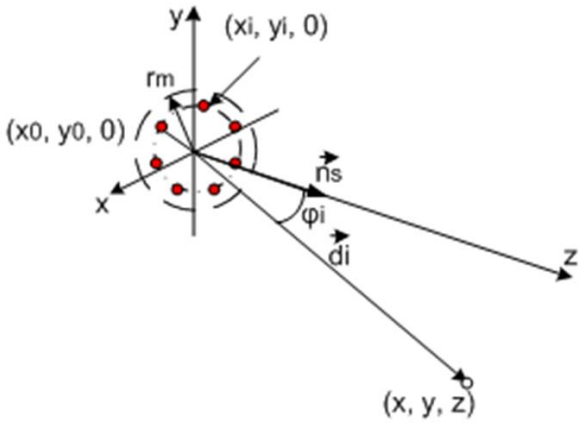

Figure 2.7 Emitting plane of discrete LEDs with circular ring arrangement [9]

Taking into consideration only one LED, for example placed in the centre of the emitting plane with coordinates (x_0, y_0, 0), and a heading of the emitting source, $\overrightarrow{n_s}$. It is possible to calculate the emitting angle, for a determined target at any point (x, y, z), given by:

$$\cos(\varphi) = \frac{\overrightarrow{n_s}.\vec{d}}{\|\overrightarrow{n_s}\|\|\vec{d}\|} \quad (2.7)$$

Where the angle is obtained from the dot product between the distance vector, $\vec{d}$, and the heading of the source. With the norm of the heading $\|\overrightarrow{n_s}\| = 1$ ($\overrightarrow{n_s} = (0, 0, 1)$), the norm of the distance is:

$$\|\vec{d}\| = \sqrt{(x - x_0)^2 + (y - y_0)^2 + (z)^2} \quad (2.8)$$

Given this geometrical setup, in fig. 2.7, the irradiance reaching on the target point (x, y, z) is given as [14]:

$$E_e(x, y, z) = \frac{m+1}{2\pi}\Phi_e \frac{cos^m(\varphi)}{\|\vec{d}\|^2} \quad (2.9)$$

That can become,

$$E_e(x, y, z) = \frac{m+1}{2\pi}\Phi_e \frac{z^m}{\|\vec{d}\|^2\|\vec{d}\|^m} \quad (2.10)$$

Where, Φ_e is the radiant flux of the emitter. Finally, the irradiance can be rewritten as:

$$E_e(x, y, z) = \frac{m+1}{2\pi}\Phi_e \frac{z^m}{[(x-x_0)^2+(y-y_0)^2+z^2]^{\left(\frac{m+2}{2}\right)}} \quad (2.11)$$

An example of an inner LED co-centric ring is showed in fig. 2.7, placed in the XoY plane with each LED having a Cartesian position of (x_i, y_i, 0). The distribution of multiple LEDs over the co-centric rings, can be given by:

$$\begin{cases} x_i = r_k . \cos\left(\frac{2\pi}{N_r(k)} i + \theta\right) \\ y_i = r_k . \sin\left(\frac{2\pi}{N_r(k)} i + \theta\right) \end{cases} \quad (2.12)$$

Where *i* is the index of a LED on a ring, since each ring has a certain number of LEDs, *k* is the ring index as there will be multiple co-centric rings in the matrix.

Considering now multiple points of radiant optical power, multiple LEDs in a single ring, with N_k being the number of LEDs on a ring and *M* the number of multiple co-centric rings. The total irradiance can be given by:

$$E_e(x,y,z) = \frac{m+1}{2\pi} \Phi_e \sum_{k=0}^{M} \sum_{i=1}^{N_k} \frac{z^m}{[(x-x_i)^2+(y-y_i)^2+z^2]^{\left(\frac{m+2}{2}\right)}} \quad (2.13)$$

Index *k* is a part of the index *i*, for the representation of the discrete LED coordinates (x_i, y_i, 0) on the XoY plane.

When the target point goes further and further away from the emitting matrix, the z coordinate increases more than the others as the LOS analysis is made mostly on the longitudinal view from the signal traffic light. What happens is that the emitting matrix of discrete points can be approximated by a single point of emission based on the central point of the circular array, due to the x_i, y_i LED discrete coordinates magnitude, is low in comparison with the target point coordinates magnitude. As the irradiance can be approximated by:

$$E_e(x,y,z) = \frac{m+1}{2\pi} \Phi_e N_{LEDS} \frac{z^m}{[(x-x_0)^2+(y-y_0)^2+z^2]^{\left(\frac{m+2}{2}\right)}} \quad (2.14)$$

Following the equations of a Lambertian radiance power source model, as described before, and using the linear approximation (obtained from the LED HLMP-EG1A-Z10DD datasheet from Avago) from the relationship between a single LED luminous intensity vs forward current, it is possible to obtain the propagated radiant intensity from the LED matrix on the normal axis. The irradiance obtained at 1m from the normal axis of the matrix is equivalent to the radiant intensity.

In fig. 2.6 and 2.8, it is showed the proposed LEDs distribution and the resulting luminous intensity vs driving current.

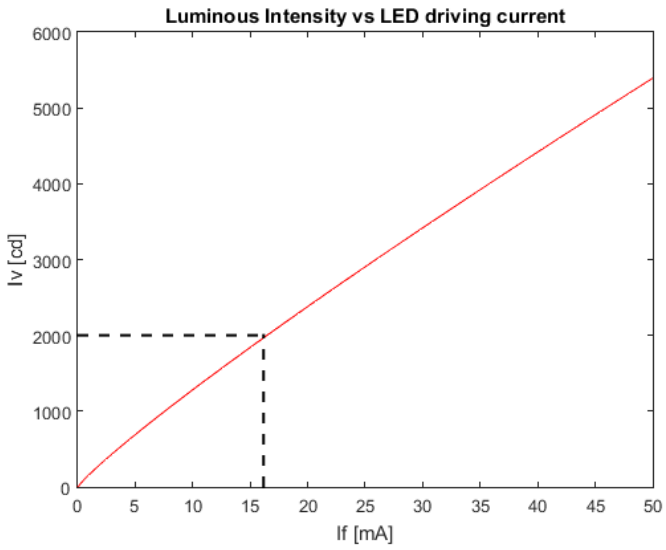

Figure 2.8 Matrix luminous intensity vs LED driving current

The simulations provide a LED distribution matrix for computed standard luminous intensity value dependent on the LED driving current, in order to evaluate the compliance with the European regulatory norms and requirements for traffic control equipment.

Table 2-2 Luminous intensities (I) for traffic signal lights over the reference axis.

Performance level	1	2	3
I_{min}	100 cd	200 cd	400 cd
I_{max} class1	400 cd	800 cd	1000 cd
I_{max} class 2	1100 cd	2000 cd	2500 cd

Therefore, the emitter physical and optical characteristics comply with:

- Diameter for signal traffic lights: round signal light with a nominal diameter of 200mm.
- Performance level class: 2/2
- Luminous intensity distribution: W (hpa=15°)

2.2.4 Receiver Model

In VLC systems there are different types of devices capable of detecting optical signals and represent them in the electronic domain. These range from digital cameras to photodiodes; digital cameras have usually a low acquiring frame rate and are used for multiple access systems or for communications systems that employ multilevel ODAC codification; in case of photodiodes there are two options avalanche photodetector (APD) and PIN photodiodes, where the latter is preferable for outdoor communications link due to the presence of high optical noise sources as APD can greatly increase the noise component with their intrinsically gain effect.

Signal reception model is of paramount importance in the description of the received signal by the optical-electronical front end. Considering the use of a PIN photodiode, this device can sense the optical power reaching its photo detection active area over a wide spectral range, usually where the visible light is included. This process is described the PD spectral responsivity, where the incident spectral power is integrated and produces a photo generated electrical current, this is usually a good measure of the device performance [1].

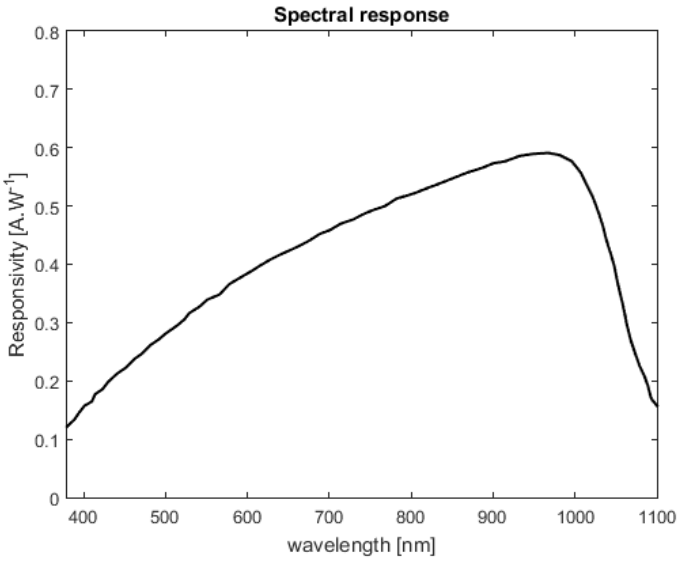

Figure 2.9 FDS100 photodiode spectral responsivity

Photodiodes based on SI junctions usually have a similar response to that of the example on fig. 2.9, based on the FDS100 from Thorlabs. Despite having a full coverage on the visible spectrum, the responsivity maximum occurs in the near IF part, where only optical noise sources will contribute with high spectral power density in this region. Due to a lack of a better choice in the photosensitive diodes industry with a better spectral response in the exclusive visible range. To solve this problem, the system could include an optical short-pass filter, like the 700SP which cuts off some of the IR interference component on the receiver, however the filter alone costs around 30 €.

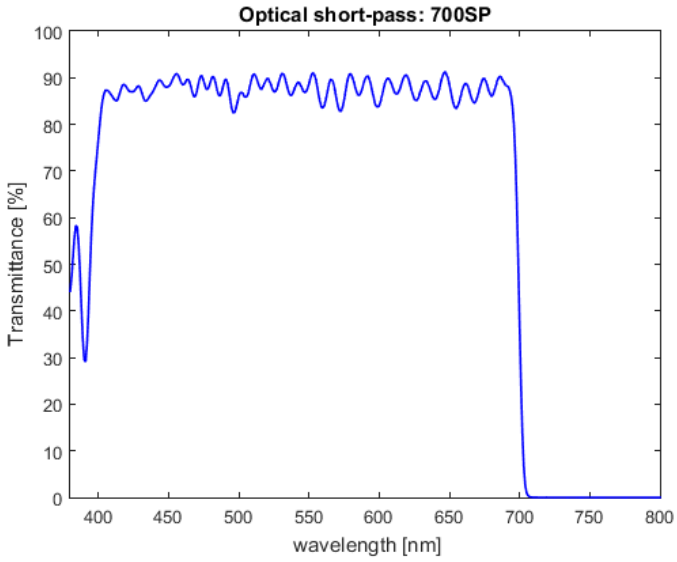

Figure 2.10 Optical band-pass filter transmittance response

Responsivity is defined as the ratio between the incident optical power and the generated photocurrent, is dependent on the quantum efficiency (η) of the sensitive material as represented in equation 2.15 [1], where q is the electron charge, λ is the wavelength, h is the Planck constant and c the speed of light.

$$\mathrm{R}(\lambda) = \frac{I_{ph}}{P_o} = \eta \frac{q\lambda}{hc} \quad (2.15)$$

$$A_{eff}(\sigma) = \begin{cases} A_d . cos(\sigma); |\sigma| < FOV \\ 0 \quad\quad\quad\quad ; |\sigma| \geq FOV \end{cases} \quad (2.16)$$

The model results in eq. 2.16, which provides the effective signal collecting area of the photo receiver, which depends on physical/geometric parameters such as the PIN active photosensitive area (A_d) and the angle of incidence (σ) of the incoming optical radiation which depends on the relative position of the receiver to the emitter. Photodetectors have a limited FOV, the incident angle of radiation must be within the limits of the detector specified by the precited parameter.

Narrowing the receiver FOV and consequently increasing its directivity towards the emitter can improve signal reception and cutting off some undesired optical background interference noise, but that would require to the emitter and receiver to be aligned, which can happen in this I2C scenario but will not be normal occurrence. To complete this model is further necessary to provide some additional information of the receiver, its position and vertical inclination respect to the normal of the road and as shown in figure 2.11.

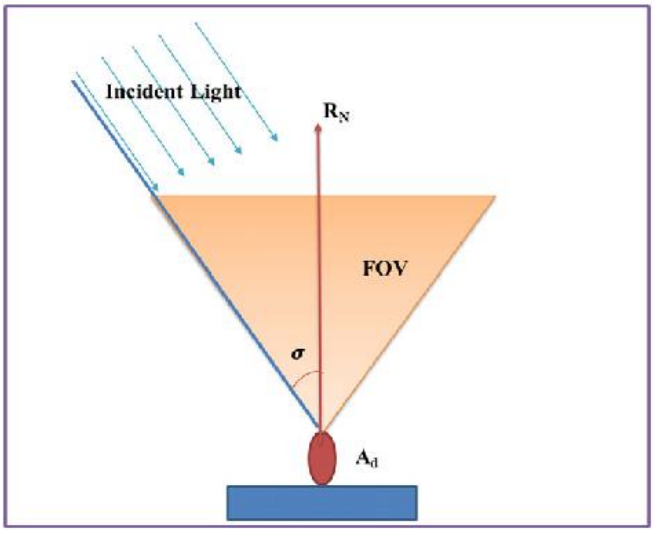

Figure 2.11 Receiver model [16]

2.2.5 I2C LOS Model Description

A simplified model for I2C communication is illustrated in fig. 2.1. After pre-processing valuable traffic data will be transmitted to oncoming cars from the signal traffic light, modulating the visible light intensity of the LED emitter. The LOS model approximates the power that reaches the receiver based on a photodetector and an amplifying stage capable of processing optical information and amplifying the signal. The parameters and the model specifications for the emitter and the receiver can be found in table 2-3, where the red traffic light must be housed on the top of the signal head, whilst standing poles of the traffic signal must be placed near the roadway, with a height comprehended between 2m to 3.5m, in accordance with the regulations decree [19].

In this model, it is assumed a traffic light position in a 3D scenario with Cartesian coordinates that define its location on the origin (0,0,h_E) and a variable position of the receiver (x_r,y_r,h_R) but with a fixed height, where *X* is the distance along the roadway width (in accordance with urban main roadways municipality regulations that specify a minimum roadway width of 7 m) and *Y* the distance along the road length (the considered or under evaluation service range). One of the major loss factors, which will be included in the LOS path gain model, is the distance between the emitter and receiver represented by the term *d* and the produced gain has an inverse square relation with the distance. This term is obtained by:

$$\vec{d} = (x_r, y_r, h_R - h_E) \quad (2.17)$$

and,

$$\left\|\vec{d}\right\| = \sqrt{x_r^2 + y_r^2 + (h_E - h_R)^2} \quad (2.18)$$

To obtain the emitting angle from the source and the incident angle on the receiver is necessary to define the heading of the source (E_N) and the heading of the receiver (R_N), these values are set with the horizontal inclination and vertical inclination respectively, on table 2-3. Recurring to the internal product definition between vectors to obtain the transmission angle (ϕ) and the incident angle (σ) can be respectively defined by:

$$\phi = \cos^{-1} \frac{(\overrightarrow{E_N}.\vec{d})}{\|\vec{d}\|\|\overrightarrow{E_N}\|} \quad (2.19)$$

$$\sigma = \cos^{-1} \frac{-(\overrightarrow{R_N}.\vec{d})}{\|\vec{d}\|\|\overrightarrow{R_N}\|} \quad (2.20)$$

Where the radiant intensity is given by [15]:

$$R_i(\phi) = P_t.\frac{(m+1)}{2\pi}.cos^m(\phi) \quad (2.21)$$

Table 2-3 Simulation Parameters

Emitter simulation parameters			**Receiver simulation parameters**		
Description	**Notation**	**Value**	**Description**	**Notation**	**Value**
Emitter half angle	hpa	15°	FOV of the PD	FOV	65°
Luminous intensity	Iv	200-2000 cd	Physical area of PD	A_d	13 mm2
Wavelength peak	λ_{peak}	626 nm	Height	h_R	1 m
Spectral Bandwidth	Δλ	28 nm	Vertical inclination	θ	80°
Horizontal inclination	φ	5°	Responsivity	R	Fig 2.8
Height	h_E	3 m			

These values can change when considering a moving receiver (x_r, y_r). Whereas E_N and R_N are the emitter and receiver normal heading with unitary norm. The emitter receiver distance, or signal traffic light to car distance is a big factor when calculating the channel loss, and consequently the signal decay increases further is the distance of the receiver in the evaluation simulation range.

2.2.6 Optical Power Path- I2C

Optical signals propagate to the receiver along two distinct conditions, one is due to the direct link between the emitter and receiver, and the other due to reflections on nearby surfaces, but as the distances involved are at least one order higher than of those indoor VLC systems, where reflections are more abundant and considerable, (the only guaranteed reflecting surface on I2C communications being the road surface) these contributions are considered insignificant face to the direct LOS optical propagation path. So this model approximates the path loss with the LOS propagation model based on the work of Ghassemlooy [15] and the signal LOS path component only suffers a linear delay between transceivers.

In the configuration represented in fig. 2.1, the radiant optical power (Watts) collected by the photodiode depends on the path attenuation factor between the traffic light and the receiver on the vehicle, the receiver model, the transmitted optical power and the relative emitter/receiver orientations. Hence the incident transmitted power is given by:

$$P_r = H_{LOS}.P_t \qquad (2.22)$$

And the complete LOS channel DC gain, depends on the transmission angle, the incident angle and the emitter receiver distance:

$$\boldsymbol{H_{LOS}}(d,\phi,\sigma) = \frac{m+1}{2\pi d^2}.cos^m(\phi).cos(\sigma).A_D.\mathcal{R}.rect\left(\frac{\sigma}{FOV}\right) \qquad (2.23)$$

In fig. 2.12, there is represented the overall power collected by photodetector over the road surface with a fixed height (h_R). This can be extrapolated from a function of the emitter spectral power of a red LED integrated over the spectral responsivity range of the receiver.

$$P_{rx}(x_r,y_r,hR) = H_{LOS}.\int_{\lambda i}^{\lambda f} \mathrm{R}(\lambda).P_t(\lambda)d\lambda \qquad (2.24)$$

The dimensional results present over the channel show a longitudinal path loss due to the distance increase and the lateral loss is due to the high directivity of the source beam but this characteristic of the emitter helps compansate the longitudinal loss. The high directivity evidenced in this case scenario is due to the low hpa of the emitter (15°), compensatting the link performance on the longitudinal range (y - range).

In figure 2.12, it can be seen a high received power loss near the beginning of the road length and even more when reaching the edge of the roadway, this is caused by the receiver being outside the LED's irradiance angle and/or the incident optical light being outside the receiver FOV. The magnitude of the received signal implies a necessary gain on the receiver side in order to recover the transmitted information, but this is not the only problem because there is also the necessity to consider and simulate the induced noise introduced by external optical sources presents on the transmission channel.

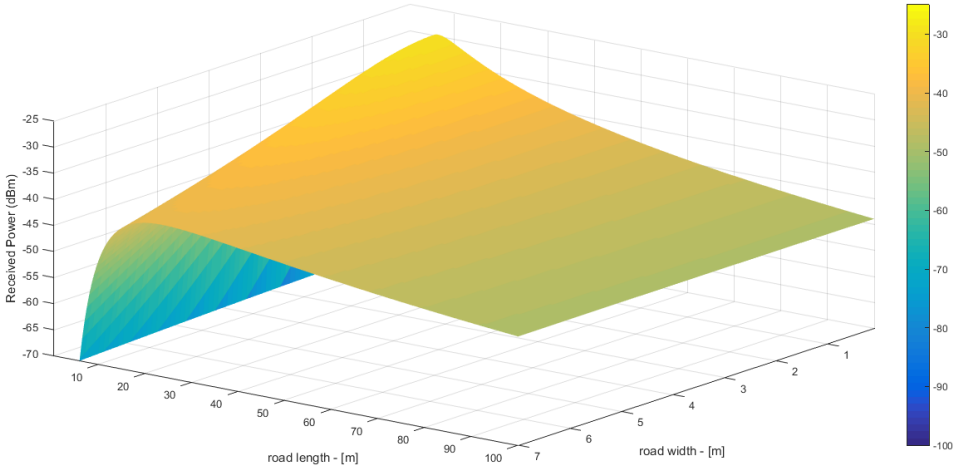

Figure 2.12 Average optical power received (dBm)

2.3 Channel Noise Sources

Outdoor VLC systems receivers are subject to intense ambient light. Having different optical background sources, depending on many factors and from all kinds of different visible light sources. The optical light sources range from artificial to natural sources of light, such as the sun, night sky radiation, street illumination, other vehicles, advertising signs and so on… These sources will generate noise at the receiver, which in turn will add to the optical signal at the receiver input, degrading the signal-to-noise ratio and therefore will be referred as optical background noise sources.

Natural light sources produce a uniform constant interference over the VLC channel, these normally can be originated by the sun and moonlight. At night the natural light irradiance main source is due to the moon's reflection of sunlight. During the day sunlight can present a constant irradiance level incident the earth's surface or considering the channel evaluation area, if there are shadowing elements present (Ex.: clouds or tree's) there will be slow variations of the irradiance intensity with time.

Artificial lights exhibit large intensity variations in time which creates an interfering signal at the receiver. This is not classified as noise because the interfering signal has a deterministic behaviour normally associated with lower band electric frequencies that can be filtered at the receiver stage. But nevertheless, artificial light also produces a DC component at the photodiode, which will generate noise.

2.3.1 Electronics Noise

Noise generated at the receiver consists of two primary components, thermal noise and shot-noise. Thermal noise is a product of thermally induce variations in resistive components. The noise voltage variance is given by:

$$V_{th}^2 = 4K_B TR \qquad (2.25)$$

Where K_B is the Boltzmann constant, T is the absolute temperature in Kelvin, B the observation bandwidth and R the load resistance at the receiver.

Optical background irradiance sources cause shot-noise at the receiver input stage. The presence of ambient light sources, with different spectral distributions and an overall spread presence in the photodetector spectral sensitivity range, contribute to noise. The average incident optical power generates a continuous photocurrent at the receiver stage, which causes Shot-noise (n(t)) to rise. Shot- noise is associated with the passage of carriers through a potential barrier, this means that any photocurrent in the photodiode will have associated noise. Shot-noise is described by a Gaussian distribution with zero mean and a white power spectral distribution.

Where the spectral density of quantum shot-noise associated with the I_{DC} current flowing through the PD p-n junction is given by [20]:

$$N_o = 2qI_b \quad \left(\frac{A^2}{Hz}\right) \tag{2.26}$$

Where q is the charge of an electron and I_b is the total DC photocurrent in the receiver. The total noise variance is then given by:

$$\sigma_n^2 = 2qI_bB \tag{2.27}$$

Where B is the baseband signal bandwidth.

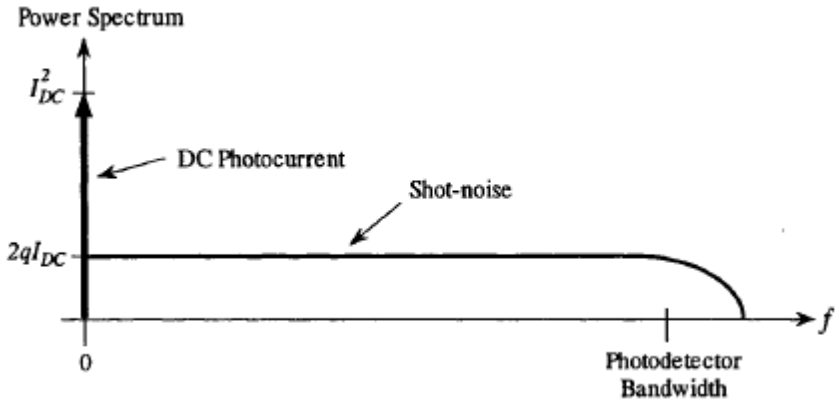

Figure 2.13 Power spectrum of a constant photocurrent on a photodetector and the noise spectral distribution [20]

In fig. 2.13, shows the spectral distribution for the Shot-noise being uniform throughout the spectrum, which is characteristic for white noise sources. The shot-noise presence can span up to the photodetector bandwidth, but a baseband signal spectral occupancy occupies a lower bandwidth, and this is the spectral occupancy range considered for the shot-noise calculations.

Note that when the optical signal power increases, with non-negative components the (I_{DCsig}) signal photocurrent generated increases, but the DC component contributing to shot-noise also rises:

$$I_b = I_{DCsig} + I_{Bg} + I_{dark} \tag{2.28}$$

Where I_{Bg} is the DC photocurrent generated by the background illuminance and I_{dark} is a small current that flows under no optical exposure. Shot-noise is the dominant noise source in OWC systems, the background current can be several times higher in magnitude when compared with the receiver signal, especially in the presence of direct sunlight [15].

The noise present at the receiver stage can be modelled as AGWN (additive white gaussian noise), in information theory this type of noise is described by: i) Additive, the noise is randomly added to the signal; ii) White, has an even power distribution along the spectrum; iii) Gaussian, because it has a normal distribution in the time domain with zero mean value.

2.3.2 Signal and Noise

In the standards developed for communications systems there are important evaluation metrics between signal and noise (S/N or SNR). In digital communication this metric developed in the form of Eb/No, which is a normalized version of SNR. Where Eb is the energy per bit and No, as referred, is the noise power spectral density. Rewriting Eb and No, respectively as:

$$E_b = P_s T_b \quad (W.s) \tag{2.29}$$

$$N_o = \frac{N}{B} \quad (W.s) \tag{2.30}$$

Where Ps is the signal power, N is the noise power and B the bandwidth. Replacing the equivalent data rate in the bit duration and establishing the Eb/No relation.

$$\frac{E_b}{N_o} = \frac{P_s}{N}\left(\frac{B}{R_b}\right) \Leftrightarrow SNR = \frac{E_b}{N_o}\left(\frac{R_b}{B}\right) \tag{2.31}$$

The equation above shows Eb/No as a normalized version of the signal to noise ratio (SNR), one of the most important tools for evaluating a system performance in digital communications and also enables an evaluation for the bit error probability [21].

In optical wireless communication systems, considering only a LOS propagation of the optical signal, the Eb/No can be expanded into:

$$\frac{E_b}{N_o} = \frac{P_t H_{LOS}(0) T_b}{N_o} \tag{2.32}$$

P_t – transmitted optical power

$H_{LOS}(0)$ – channel DC response loss

The electrical SNR version, considering a majoring source of noise as Shot-noise and taking into consideration the electrical signal power generated at the optical receiver.

$$\frac{E_b}{N_o} = \frac{(P_t \mathcal{R} H_{LOS}(0))^2}{2qI_b R_b} \quad (2.33)$$

2.3.3 Black Body Radiation

The most common light source comes from the radiation emitted by thermally excited atoms, in the form of solid or gas bodies, as in the case of the Sun or incandescent lightbulbs. When considering a perfect emitter (black body) heated to an absolute temperature T, its spectral radiance can be empirically described by Planck's law [22]:

$$P(\lambda) = \frac{2\pi c^2 h}{\lambda^5 (e^{hc/\lambda kT} - 1)} \quad (2.34)$$

According to this expression, the emitting body radiation spectrum presents a continuous behaviour (fig. 2.14) with an emittance peak at a certain wavelength (λ_m), which is inversely proportional to the body's temperature. This relation describes the radiance from infrared to ultraviolet spectrum.

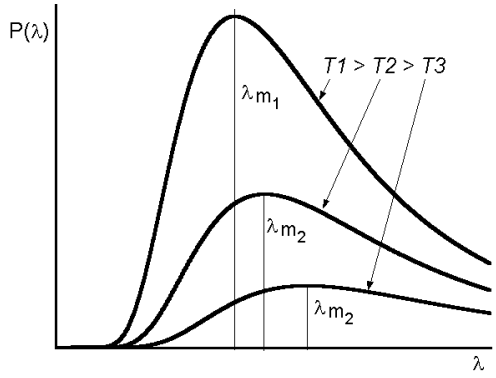

Figure 2.14 Black body emission spectrum varying with temperature [41]

- Sunlight: High irradiance from the sun at earth surface level, producing high levels of photocurrent at the receiver. The level of irradiance is not constant and highly dependent on external factors of a VLC channel. In order to produce a complete model we need to contemplate several factors; such as time of the year (which changes with the earth sun mean distance), geographical location (latitude) and the vertical altitude of the sun (which

also changes along the day)[22]. The sun radiates isotropic radiation with a spectrum approximated by its photosphere temperature 5780 Kelvin, the region generating light [23], on fig. 2.14 it can be observed the sunlight's PSD upon the photodiode sensitivity range.

- Moonlight: Moon's radiance on the earth's surface caused by the reflection of the sun on this natural satellite is affected by a number of elements and variables [22] - the phase of the moon, the earth-moon distance variation, the differences in reflectance (albedo) surfaces in the moon, the relative altitude of the moon in relation to the horizon line and the weather conditions.

  The moon as spectral radiance can be approximated by a blackbody radiation at 4100 Kelvin [24], in fig. 2.15 there is an example for the moonlight's approximated spectrum from 0.38µm to 1.1 µm.

- Artificial lights:
  - the incandescent light source produces light, in which this process involves resistively heating a tungsten filament inside the bulb with a current conducted through it. The tungsten filament heats up to around 2900 Kelvin when a steady state of operation occurs, and the modelled spectrum of radiation is a black body around that temperature. A lot of the radiated energy from these lightning sources also have a very strong component in the near IR of the spectrum in which visible light photodetectors have a strong responsivity.

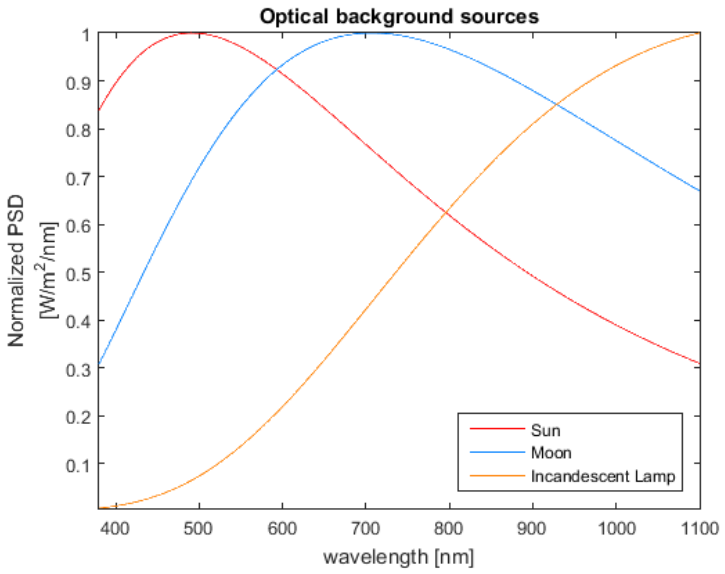

Figure 2.15 Normalized PSD from natural and artificial optical sources

Fig. 2.15, displays the normalized power spectral distributions of different light sources, with the spectral window scaled to the receiver sensitivity range. As it can be seen the Incandescent lamp as a stronger component in the infrared region of the spectrum due to their low efficiency and high radiation heat generation, whereas the sunlight radiation has a stronger component in the ultra-violet region.

3. Chapter 3

When developing an OWC system one of the most important factors is choosing an appropriate type of modulation technique to enhance the system's performance, depending on the requirements for the link setup. Many of the existing VLC modulation techniques are based in radio and infrared technical backgrounds. The optical characteristics in a visible light emitter differ significantly from RF systems. In radio, proprieties of the carrier wave like amplitude, frequency and phase can be modulated by the transmitting data, whereas in VLC is only the intensity of the optical carrier, usually LED radiant power propagating in multiple directions which is a real nonnegative value, that can be modulated. LEDs are an incoherent light source, they emit light with multiple changes in phase and frequency [17]. The generation of light comes from the transition of an electron in high energy state to a lower state, the energy bandgap between these two levels is directly correlated to the frequency/wavelength of the emitted photon.

This chapter presents some basics around different types of visible light modulations and circuit approaches. Limitations and requirements that influence various aspects, such as bit rate vs bandwidth limitations, modelling error performance and power efficiency.

3.1 VLC Impairments

When designing the VLC system, there are some requirements over practical impairments to consider for the optical signal propagation. There are eye safety regulations [25] to comply with in terms of optical power. VLC emitters do not emit focused beams, such as LASER's, which can cause possible damage to the eye. However, due to our "high sensitivity" to visible light there is an adequate limit on the mean optical power propagated by the emitter, but not as much as in IR communications.

Another concern in VLC systems is maintaining a "constant" light intensity, whistle varying the emitter intensity. Fast switching features, necessary for data communication are not always suitable for that purpose, since mean light intensity could change with the bit probability. To avoid this, there are some line codes such as Manchester, which maintain a mean DC value independently of the symbol to convey, thus levelling a constant light output at the emitter.

3.1.1 Channel Bandwidth Limitations

As referred before multipath dispersion will not be included for the I2C simulations, it is only considered the LOS propagation. Multipath dispersion will be a subject addressed in chapter 5 with the C2C scenario.

Signal bandwidth limitations can be from different elements in the communication system, like the receiver configuration or the emitting LEDs.

The emitting LEDs do not have an infinite bandwidth, this is one of the major limitations for high data rates in VLC systems. The recombination dynamic processes inside the semiconductor junction are limited by the minority carriers' lifetime, which limits the time between the transitions of the LED on and off state. This process defines the optical bandwidth of the emitting device, which occurs when the parasitic junction capacitance starts pulling the driving current down, [17]. In table 3-1, there is a list of tested LEDs for their optical bandwidth, with the respective maker, model, colour and bandwidth in MHz.

Bandwidth measured with OOK modulation and LED response times [5][26]:

Table 3-1 Different LEDs modulation bandwidth

Manufacturer	Model	Colour	I_F (max) [mA]	Optical Bandwidth [Mhz]	Switching Time [ns]
OSRAM	LA W57B	Amber	400	3.10	
	LY W57B	Yellow	400	4.10	
	LV W5SG	Green	500	8.70	
	OSLON SSL 80	White	800	3.0	
VISHAY	TLMK3100	Red	30	8.30	42.11
	TLCR5200		50	7.50	46.63
	TLCR5100		50	7.23	48.35
	TLCR5800		50	7.50	46.63
	TLCY5100	Yellow	50	5.89	59.38
	TLCY5200		50	8.04	43.52

	TLCY5800		50	5.89	59.38
	TLCTG5100	Green	30	6.53	53.54
	TLCTG5800		30	8.04	43.52
	TLCTG5200		30	7.5	46.63
	TLCB5100	Blue	30	11.75	29.76
	TLCB5200		30	12.16	28.75
	TLCW5100	White	30	2.40	
	TLMW310		20	2.40	
Nitchia	TLMW3100		20	2.40	145.94
	NSPW500BS		30	2.57	136.20
Multicomp	OVA-1033	Blue	30	9.9	
	OVA-1031	White	30	2.8	
	OVA-1031	White w/ blue filter	30	3.45	
TT Electronics	OVLFR3C7	Red	50	5-6	

The results present in table 3-1, are a collection of different sources and work developed in Integrated Systems and Circuits group from IT Aveiro, where the last entry on the table was made from an experimental setup and measurement develop in this work.

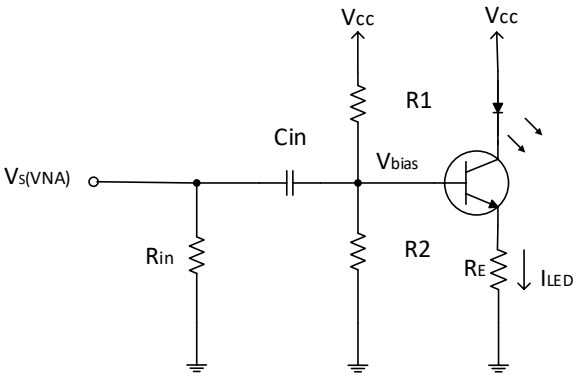

Figure 3.1 Voltage mode emitter circuit

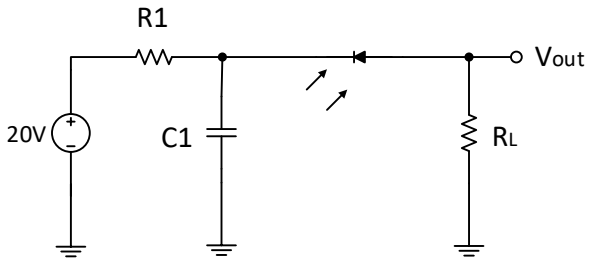

Figure 3.2 Receiver circuit

The experimental setup consisted in a transmitting LED at a distance of 2 cm to the receiving photodiode, the system bandwidth was measured by using a VNA (vector network analyser) where port 1 was connected to the emitter and port 2 was connected to the receiver. The bandwidth was obtained by getting S21 parameter magnitude. The adaptation circuits required for driving the LED and photodiode polarization, are represented by fig. 3.1 and fig. 3.2 respectively. The LED driving is accomplished by using a bipolar transistor, in a common emitter configuration with the LED in series with the transistor collector. The resistor on the emitter, R_E, sets the current on the LED, given by:

$$I_{LED} = I_{bias} + I_s \quad (3.1)$$

Where I_{bias} is the DC bias current and I_s the signal current driving the LED both established by:

$$I_{bias} = \frac{V_{cc}\frac{R_2}{R_1+R_2} - V_{be}}{R_E} \quad (3.2)$$

$$I_s = \frac{V_s - V_{be}}{R_E} \quad (3.3)$$

The optical receiver is a reversed biased photodiode, with an input noise filter, implemented by R1 and C1. The bias voltage was set to 20V, which according to the datasheet provides a junction capacitance, C_j, of 24pF. The receiver bandwidth is given by:

$$BW = \frac{1}{2\pi C_j R_L} \quad (3.4)$$

With a load resistance, R_L, of 50 ohms the implemented receiver bandwidth is approximately 132.6MHz. Since the expected LED bandwidth is around few MHz, this limitation has a small impact on overall system bandwidth.

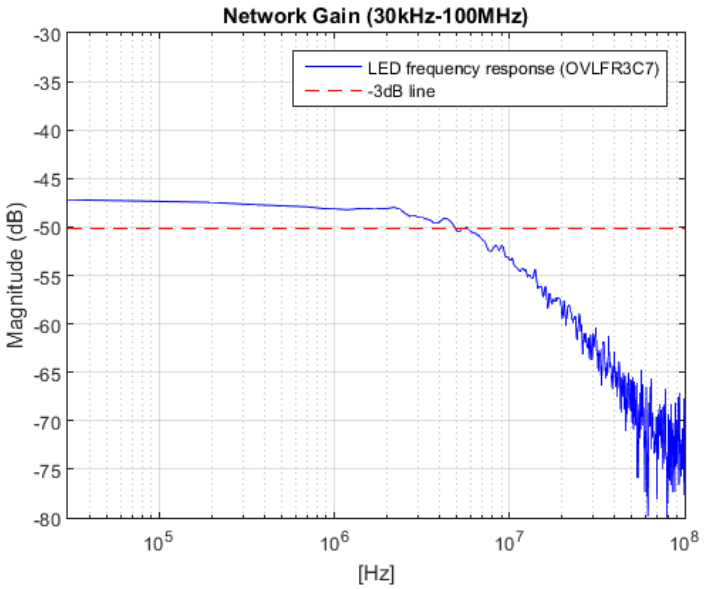

Figure 3.3 Measured optical bandwidth of OVLFR3C7

The measurement results in fig 3.3, were made on VNA. The cut off frequency relation can be given by:

$$|H(f_c)| = \frac{H(0)}{\sqrt{2}} \quad (3.5)$$

Being,

$$H(f) = \frac{V_{out}(f)}{V_i(f)} \quad (3.6)$$

Analysing the data obtained from the VNA measurements, the expected LED optical bandwidth was according to other research measurements on LEDs. Optical receiver bandwidth limitations are not of high concern, due to the existence of other architecture configurations with lower load impedances [27], increasing even further the available receiver bandwidth.

3.2 Digital Baseband Modulations

The purposed modulation schemes are included in this class, of baseband modulation, where the data/symbol transmission is not shifted to a high carrier frequency before the intensity modulation of the optical source. After modulation being applied to the transmitted data a line code can constrain even more the transmitted signal shape. Line codes usually provide some advantages which can range from clock recovery to facilitate synchronization, to capability of error detection and correction. The generated and transmitted signals in visible light applications after modulation have a strong DC component in their power spectral distribution analysis, this is due to optical signal generated, can only be considered bipolar with a DC offset, being its amplitude ranging only in positive values. All optical visible light modulations optical signals can be considered unipolar.

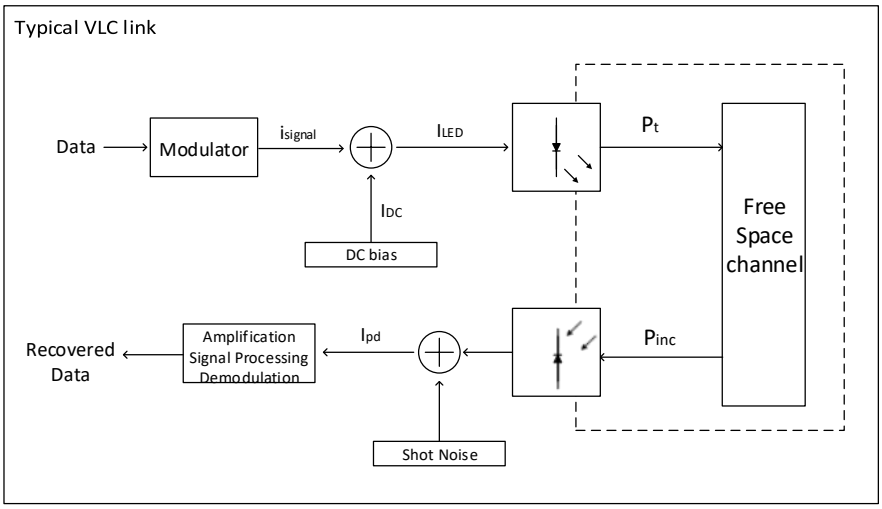

Figure 3.4 Typical VLC block diagram

Fig 3.4 represents a typical VLC system setup with main blocks for the emitter and receiver stages, in the emitter it is displayed the DC bias point applied to the emitting LEDs at which is added the modulated signal. The transmitted optical signal has a DC component based on the DC current bias point of polarization.

In on-off keying modulation with non-return to zero (OOK-NRZ) of a light source, the optical signal is in the form of a rectangular pulsed shape. In the time domain the rectangular pulse can be given by:

$$x(t) = rect_T(t) \quad (3.7)$$

The power spectral distribution of the rectangular function with pulse width Ƭ is given by the Fourier transform of the time domain signal and is approximated by [28]:

$$X(f) = AT\frac{\sin(\pi Tf)}{\pi Tf} \quad (3.8)$$

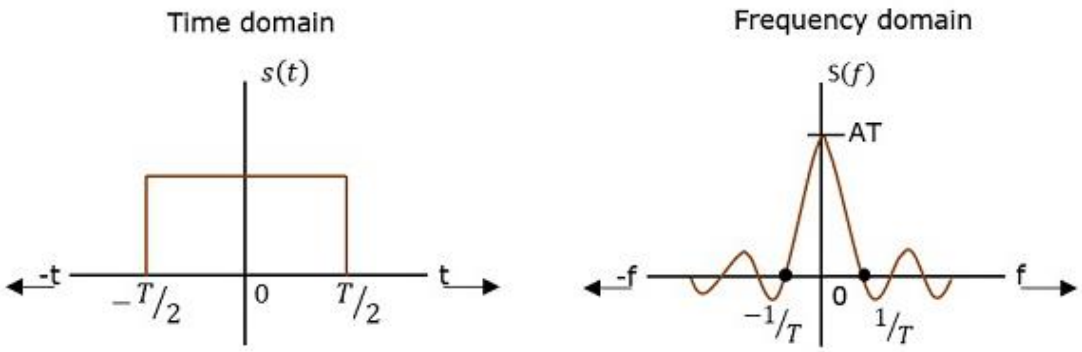

Figure 3.5 Rectangular pulse shape and PSD of the Fourier transform [28]

Which is the sync function represented in figure 3.5, also in this figure is represented the rectangular pulse shape typical of OOK-NRZ modulation scheme. The data rate R_b (bits/s) is inversely proportional to the pulse duration Ƭ and as the bandwidth occupancy is between the DC point up to the first null in the PSD of the transmitted signal, the bandwidth B is also inversely proportional to the pulse duration. Which gives the theoretical spectral power efficiency for OOK-NRZ to be limited to 1 (bit/s(Hz) and considering the LED pole, this can turn into a major limitation to data rate transmission in visible light systems.

3.2.1 IIM – Impulse Intensity Modulation – DD – Direct Detection

LEDs emitting non-coherent light do not enable a lot of modulation options as RF does (phase and frequency combinations), so usually modulation of optical power is made recurring to intensity modulation (IM) and direct detection (DD). Modulated information drives the forward current in the LED emitter or LED emitting arrays, controlling the proportional radiant optical power propagation within the linear O-I (optical-current) curve by the driving signal. The modulation driving should be mapped in the LED linear current range [29], two much driving amplification may incur in high non-linear distortion of the optical signal. Limitations on the optical power driving amplitude favour modulations with high peak to average power ratio (PAPR) such as OOK, PPM or DPIM, but can have a crippling effect on the performance of multilevel and/or multicarrier modulation schemes such as PAM (pulse amplitude modulation), OFDM (orthogonal frequency division multiplexing) and or CAP (carrier less amplitude phase).

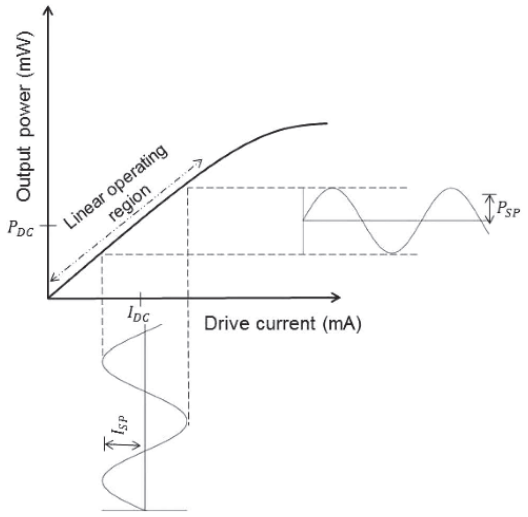

Figure 3.6 Current to optical output behaviour [29]

As shown in figure 3.6 the linear behaviour of the modulation mapping will produce a linear signal propagated in the optical domain and a constant DC bias polarization will maintain a constant light intensity output. The average transmitted optical power, over time can be given by:

$$P_t(t)) = P_{DC} + P_{signal}\,, P_{signal} = mP_{DC} \quad (3.9)$$

Where *m* is the modulation factor that describes the current modulation mapping. The wavelength dependent optical power can be described by:

$$\begin{cases} I_F = I_{DC} + i_{sig} \\ P_t(\lambda) = \eta(\lambda) I_F \end{cases} \quad (3.10)$$

The electro-optical efficiency (η(λ)) also includes the wavelength width distribution of the emitting red LED, as LEDs are not a monochromatic light source [17].

On-off-keying (OOK) modulation is one the most common example for an intensity modulation scheme applied in VLC. The LEDs are turned “on” and “off” depending on the transmitted bits being sent, bit ‘1’ for ON state and bit ‘0’ for OFF state. While logically the modulation turns ON and OFF the emitting light it does not necessary imply commuting between these two states; rather the intensity of the light may be simply reduced, as long as the two states are distinguishable in the receiver. In OOK-NRZ the pulse intensity is maintained through the bit duration.

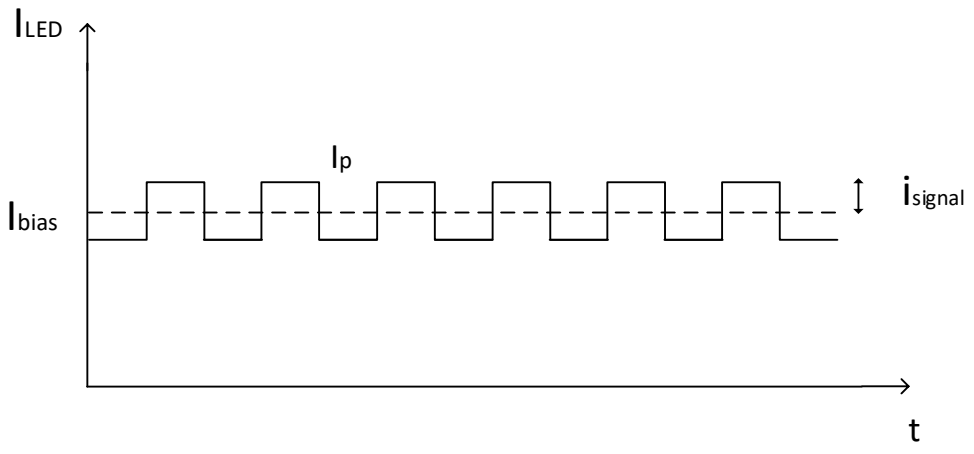

Figure 3.7 On-Off intensity modulation of a LED forward current

An example of the modulated electrical signal plus bias point, fig. 3.7, depict being similarly to a clock line with an offset, it represents alternating 1's and 0's being sent. This shows the current driving a LED controlling the transmitted optical power, where the driving mapping occurs around the bias point.

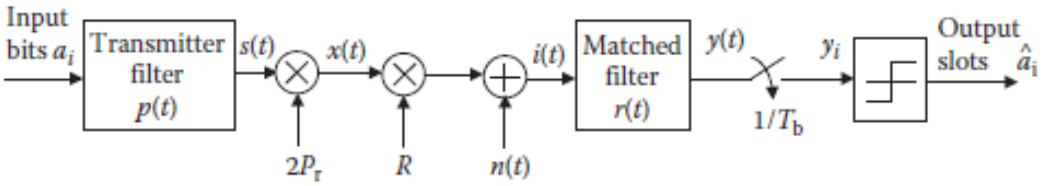

Figure 3.8 Block diagram of OOK system architecture

In the proposed transmission scenario, fig. 3.8 [1], an additive white Gaussian noise (AWGN) channel without distortion, the optimal maximum likelihood receiver for OOK-NRZ, is a matched filter fitted to the transmitted pulse shape, followed by a sampler ADC and a threshold detector. Considering the same probability of receiving ones and zeros, the threshold level is midway between the two levels. The bit error probability for OOK-NRZ modulation scheme is given by [1]:

$$BER_{OOK-NRZ} = Q\left(\sqrt{\frac{E_b}{N_o}}\right) \quad (3.11)$$

Q is the error function, defined by,

$$Q(x) = \frac{1}{\sqrt{2\pi}}\int_x^{\infty} e^{-\frac{y^2}{2}}\,dy \quad (3.12)$$

The average energy per bit E_b is given by

$$E_b = \frac{E_p}{2} = \frac{(mP_{inc}\mathcal{R})^2}{R_b} \quad (3.13)$$

It was assumed an average received optical power with a DC component of P_{inc}, a photodetector responsivity of $\mathcal{R}$ and the modulation mapping factor '*m*'. The current peak at the output of the receiver stage, considering only the AC component is, $I_p=2mP_{inc}\mathcal{R}$, but as the bit pulse in OOK-NRZ has half the amplitude of the current peak, the average energy at the matched filter output is estimated by:

$$E_p = \begin{cases} i_p^2 T_s; & '1' is\ sent \\ 0 \quad ;' & 0' is\ sent \end{cases} \quad (3.14)$$

The ratio Eb/No is the reference value of digital optical communications in terms of SNR development and it is widely used for developing the value of the performance factor BER.

$$\frac{E_b}{N_o} = \frac{(mP_{inc}\mathcal{R})^2}{2qR_b I_b} \quad (3.15)$$

3.2.2 PPM Modulation

Pulse position modulation is an orthogonal modulation and as the name infers is a pulsed based type of modulation. A symbol information is coded into the pulse position within L number of slots, being transmitted a pulse in the slot position corresponding to the symbol. Each frame transmits M bits or $\log_2$ (L) bits and this modulation has a fixed frame duration of LT_{slot} (T_{slot} – slot duration). To have the same data throughput as OOK-NRZ, T_{slot} duration has to be shorter than OOK bit duration [1].

$$T_{slot} = T_b \frac{M}{L} \quad (3.16)$$

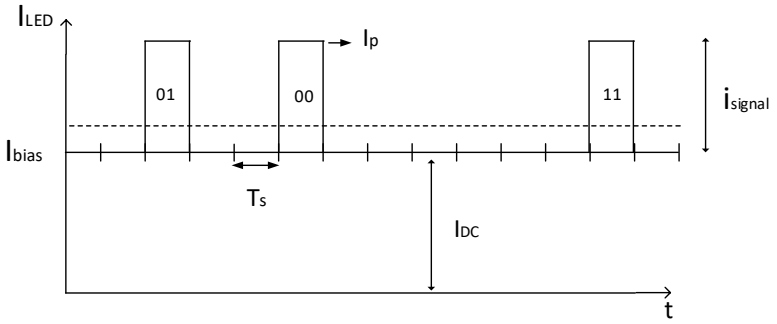

Figure 3.9 4-PPM waveform

The above figure shows an example of 4-PPM, where each symbol transmits 2 bits. The example is representing also the LED driving current with a current peak proportional to the symbol length. Pulse based modulations enables a higher average peak to average power ratio and in order to maintain an average optical power being transmitted as the ratio between pulse slot and empty slots being 1/L. But as the power efficiency improves, the bandwidth efficiency does not. PPM

modulation bandwidth occupancy is approximately L times larger than OOK-NRZ. To maintain a mean optical power requirement the driving pulse amplitude is given by:

$$I_p = mI_{DC}\sqrt{L} \quad (3.17)$$

Note that there are several practical limitations to optical power and driving amplitude in a LED, so a more conservative scaling of the L factor should be considered, in order to avoid reaching the LED maximum driving current.

The receiver for PPM requires both slot and symbol synchronization, it is more complex than an OOK receiver. However in an AWGN channel with a threshold detector with detection level midway level between amplitude pulses the slot error probability (P_{sle}) can be approximated by [15]:

$$P_{sle} = Q\left(\sqrt{\frac{E_s}{2N_o}}\right) \quad (3.18)$$

Where E_s is the average energy per symbol, with M bits of data, the average energy per symbol is given by:

$$E_s = E_b M = M(mP_{inc}\mathcal{R}\sqrt{L})^2 T_{slot} \quad (3.19)$$

The energy per bit is estimated by the amplitude power at the input of the matched filter, which is dependent on the driving factor, and the higher PAPR of the PPM modulation scheme. The probability of slot error can be converted into the symbol error probability by using:

$$P_{sye} = 1 - (1 - P_{sle})^L \quad (3.20)$$

Considering also equal probability for each symbol, the corresponding BER is given by:

$$BER_{PPM} = \frac{L/2}{L-1} P_{sye} \quad (3.21)$$

3.2.3 DPIM Modulation

Differential pulse interval modulation is an asynchronous modulation. The symbol duration is different for each symbol. It consists of a pulse of a one T_{slot} duration followed by several empty slots. The number of empty slots between pulses depends on the coded information. Comparing this modulation with PPM, DPIM offers a significant increase in data throughput by eliminating the unused time slots from within each pulse [1] and as each symbol is initiated with a pulse it makes it easier to recover symbol synchronization at the receiver.

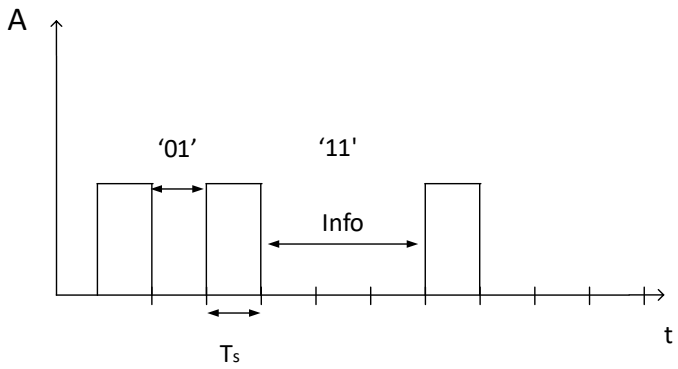

Figure 3.10 DPIM waveform

In the fig. 3.10, there is an example of the 4-DPIM waveform with the variable symbol duration, with k empty slots between pulses. This example shows no guard slot (GS), so the transmission of the '00' symbol is two consecutive pulses. With no GS the minimum and maximum symbol duration for L-DPIM is T_{slot} and LT_{slot}, respectively, and an average slot number being $L_{avg}=(L+1)/2$ [15].

To normalize to the same overall data rate of previous modulations, the average slot duration is given by:

$$T_s = \frac{M}{L_{avg}} T_b \qquad (3.22)$$

The transmitted optical power is also variable with the different symbols being sent, but in order to average the "visible" optical power the pulse amplitude being transmitted is scaled to the average symbol length. The pulsed optical amplitude can be approximated by:

$$P_p = P_o m\sqrt{L} \quad (3.23)$$

At the receiver, the optimal receiver is a matched filter followed by a threshold detector. Where the slot energy at the filter input can be approximated by the incident optical power:

$$E_s = L(mP_{inc}\mathcal{R})^2 T_s \quad (3.24)$$

In an AWGN channel with the threshold at mid-level, the slot error probability for DPIM with no guard slot is given by:

$$P_{sle} = Q\left(\sqrt{\frac{LM}{2L_{avg_{dpim}}}\frac{E_b}{N_o}}\right) \quad (3.25)$$

In the case of DPIM, a single pulse detection error can have a negative impact on decoding the following symbols/bits of the packet (symbol frame dependency reset between packets), severely degrading BER [15]. The packet error rate can be a better tool in terms of evaluating the DPIM performance, as well as for the next proposed modulation scheme. The PER (P_{er}) can be derived from the SER (P_{sle}) as shown below:

$$P_{er} = 1 - (1 - P_{sle})^{N_{pkt}L_{avg_{dpim}}/M} \quad (3.26)$$

Which depends on the N_{pkt} the number of packet bits.

3.2.4 DH-PIM Modulation

Dual header pulse interval modulation is more complex than the other modulation techniques, as DPIM it has a variable symbol length and the header slot has two types of duration pulses. The header 1 (H1), the initial pulse, with width α/2 (α is a positive integer) slot duration is followed by an (α/2) +1 protection time slots. For header 2 (H2) pulse width is α time slot, followed by one protection time slot. If the most significant bit (MSB) of the symbol data input is a '0' bit, then H1 is used and if it is a '1' bit, then H2 is used to start the symbol frame. The rest of the symbol frame, k empty slots, representing the decimal value of the input code word if the symbol starts with H1, if it starts with H2 the rest of the symbol frame represents the 1's complement decimal value of the input word. The type of header pulse used plays a dual role of frame initiation and time reference for the succeeding frames, as in DPIM scheme, removes the redundant time slots following the pulse of PPM modulation, but it also reduces the average frame duration to half of the DPIM symbol frame and statistically to a quarter of PPM, thus enabling higher data rates [30].

Where the average symbol length L_{avg} and slot duration T_s are given by:

$$L_{avg_{dhpim}} = \frac{(2^{M-1}+2\alpha+1)}{2} \quad (3.27)$$

$$T_s = \frac{2MT_b}{(2^{M-1}+2\alpha+1)} = \frac{MT_b}{L_{avg_{dhpim}}} \quad (3.28)$$

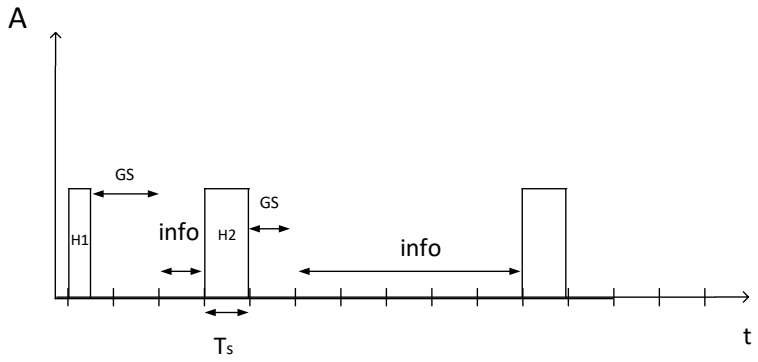

Figure 3.11 DH-PIM (alpha=1) waveform

Fig. 3.11 shows the DH-PIM pulse train, with α=1, it shows the relative pulse width to the slot duration depending on the header type.

The error performance on Gaussian channels is simulated with the receiver being composed of a matched filter, followed by a sampler synchronized with the time slot rate and ended with a threshold detector. Assuming the same optical power received at the matched filter input stage, as in PPM and DPIM, and assuming equal occurrence of H1 and H2. The energy of a pulse at the matched filter output is given by:

$$E_p = A^2 T_s \quad (3.29)$$

Therefore, the pulse energy is:

$$E_p = \frac{L(mP_{inc}\mathcal{R})^2 M \mathrm{T}_b}{L_{avg_{dhpim}}} \quad (3.30)$$

With the threshold detection set to the mean level value, the slot error probability is given by:

$$P_{sle} = Q\left(\sqrt{\frac{LM}{2L_{avg_{dpim}}}\frac{(mP_{inc}\mathcal{R})^2}{N_o}}\right) \quad (3.31)$$

The concept of bit error rate it is not easily applied to an anisochronous modulation scheme, such as DH-PIM, there are certain errors that not only effect a specific symbol frame but also shifts pulse positions of the following frames. In alternative the concept of packet error rate (P_{er}) can be used when evaluating the performance of DH-PIM.

$$P_{er} = 1 - (1 - P_{sle})^{N_{pkt}L_{avg_{dhpim}}/M} \quad (3.32)$$

Which depends on the N_{pkt} the number of packet bits.

3.3 Modulations Comparison

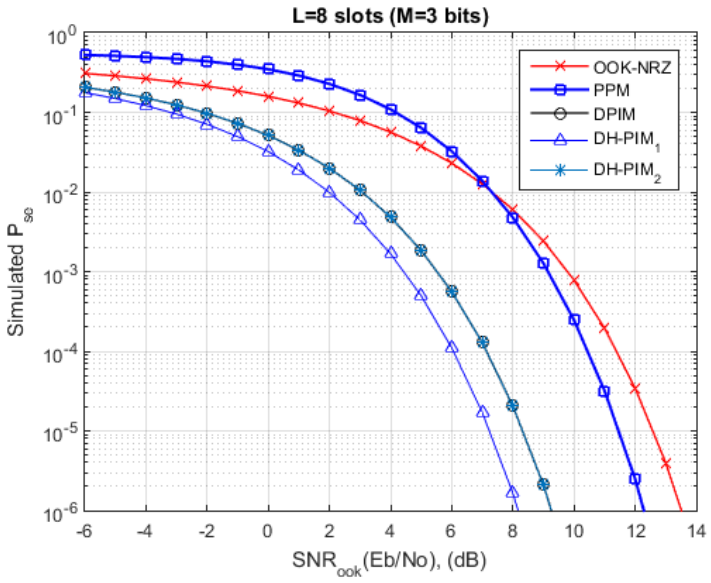

Figure 3.12 Slot error rate for OOK, PPM, DPIM and DH-PIM (α=1, α=2) versus SNR

In this work anisochronous and isochronous types of modulations, DPIM, DH-PIM, PPM and OOK-NRZ, are adopted due to their simplicity and good performance in power and bandwidth efficiency [1].

Fig 3.12 shows these modulations performance versus the signal to noise ratio, with symbol slot length, L=8, for pulse-based modulations. In the simulated results, 8-PPM achieved the optimal performance of 10^{-6} probability of error, for lower values of SNR than the benchmark scheme of OOK. Between the anisochronous schemes, DH-PIM$_1$ presented the best results reaching a target of 10^{-6} slot error at approximately 8dB of SNR.

4. Chapter 4

4.1 Variable Ambient Optical Conditions on System Performance

This chapter explores the performance of different modulation schemes under the constraints of different optical interference scenarios with constant AWGN (additive white Gaussian noise) induced in the receiver front end. For optical interference characterization it will include the measurements made from natural and artificial light sources and their power spectral distribution over the sensibility range of the photodetector. Models for the illuminance (lm/m^2) distribution and corresponding irradiance (W/m^2), for point light sources are introduced with an impact evaluation on communication evaluation metrics, like the signal-to-noise ratio, the bit-error-rate or slot-error-rate. The performance of OOK-NRZ, PPM, DPIM and DH-PIM in the presence of AWGN is investigated and the results obtained from simulation are shown in this chapter.

For the different simulation scenarios some assumptions and considerations had to be made for error analysis in all the modulations schemes under scope, these considerations are described below [15]:

- The transmission link is in line of sight and the free space channel only induces a negligible linear delay without multipath dispersion only occurring channel attenuation. The emitter height, direction and the receiver upwards orientation minimize reflection contributions from the road surface, that is, Line of Sight is the main path between transmitter and receiver.
- Noise associated with the receiver front-end components (thermal noise) is negligible and the main noise source is shot noise mainly originated by background optical radiation, which is assumed to be white Gaussian noise.
- Artificial light optical interference AC component is removed by the initial filter stage at the receiver, without much loss to the signal energy baseline, due to the artificial AC component being near DC in comparison with the transmitted signal frequency range.
- Channel bandwidth limitations are dependent on the LED optical bandwidth.

4.2 Ambient Noise Characterization

In a VLC link between the signal traffic light and car (I2C) an uncountable number of factors can influence the physical link. The received optical signal changes with the position of the car on the road lane and the service link time span is limited. In a worst-case scenario when the signal is green, a car travelling towards the emitter at an average 50km/h, with link established at 40m from crossing the signal traffic light, this would average a link span of $t_{link}= d_{link}/v_{car}$ approximately 2.8 seconds. The data link reach is not static, it can vary accordingly with the ambient conditions of the channel. The VLC link begins at a distance x and ends when the car/receivers crosses the traffic signal light line, it can happen before the said cross of the traffic light, as at near distances the optical signal propagation can be outside the detectability FOV of the receiver. The ambient light present at any time is also an important factor, due to generation of noise at the receiver.

The ambient interference is dynamic, changing from location to location depending on time of the year, geographical latitude (influence in sun intensity at earth's surface), weather conditions and time of day. In the scope of this study there are three proposed types of ambient light noise scenarios, to make a broad enough scope of the conditions described, these scenario cases are discrete cases when compared to a broader continuum but useful to emphasize worst case scenarios in different natural occurring conditions.

4.2.1 Low optical natural light

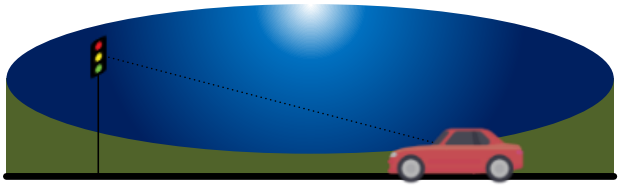

Figure 4.1 Night sky irradiance scenario on I2C VLC link

This scenario aims to predict the influence of natural light present during the night, the irradiance of the night's sky on the surface of the Earth, depicting an ideal scenario for communication to occur between infrastructure to car as no other optical source nearby is considered to exist. This interference scenario is modelled by values of illuminance levels at earth's

surface as a function of the lunar altitude angle, these values assume a clear sky with a mean earth-moon distance [22]. There are other stellar sources of illuminance from the night sky, but only provide a quarter of the illumination without considering the Moon, being this body the main responsible for natural night ground level illuminance at Earth.

Table 4-1 Full Moon Earth's surface illuminance

Electro Optics Handbook	
Moon's Illuminance on Earth's surface	
lunar altitude angle	E_v [lux]
0º	1.57e-3
10º	23.4e-3
20º	58.7e-3
30º	0.101
40º	0.143
50º	0.183
60º	0.219
70º	0.243
80º	0.258
90º	0.267

The irradiance power along the channel is uniform, the position and FOV of the receiver will not be a factor on the incident optical power from this ambient light source. The optical background power irradiance, $E_e(\lambda)$, estimated by the full-moon illuminance level (E_v) at ground level.

The black body radiation was introduced to model complex spectral sources, like the moon, and provides low complexity, and accurate results. The moon spectral irradiance (in $W/m^2.nm$), can be approximated by the equation at 4100 Kelvin:

$$E_e(\lambda) = S_p \frac{W(\lambda,4100)}{\max[W(\lambda,4100)]} \quad (4.1)$$

Where S_p is the peak of the spectral irradiance. Using the photometric-radiometric conversion and the spectral power distribution of the Moon's reflectance radiation of the solar light, the irradiance peak is given by:

$$S_p = \frac{E_v}{K_m \int_{\lambda 1}^{\lambda 2} E_0(\lambda) V(\lambda) d\lambda} \quad (4.2)$$

Where $E_0(\lambda)$ is a dimensionless spectral distribution function, representing the optical source. This parameter is given by:

$$E_0(\lambda) = \frac{W(\lambda,4100)}{\max[W(\lambda,4100)]} \quad (4.3)$$

The background DC current produced by the night's sky irradiance at the photodetector can be given by:

$$I_{moon} = A_d \int_{\lambda i}^{\lambda f} E_e(\lambda)\, \mathcal{R}(\lambda) d\lambda \quad (4.4)$$

Where A_d is the photodiode active area, $\mathcal{R}(\lambda)$ is the spectral responsivity and the integral limits the spectral sensitivity range of a silicon photodetector.

The signal to noise ratio simulations can be modelled by with the shot-noise induced by the DC photocurrent, I_b, generated at the receiver:

$$SNR = \frac{(P_{sig}\mathcal{R})^2}{2qR_b I_b} \quad (4.5)$$

Where,

$$I_b = I_{moon} + I_{DCsig} + I_{dark} \quad (4.6)$$

The total photocurrent also comes from the optical DC component of the emitter.

Two types of variations are included in the simulations, firstly the LED injected current, and consequently the traffic light average driving current, was varied inside a limited range, due to optical power regulations [31]; secondly there was another approach where the horizontal distance between the transmitter and receiver varied from 0 to 100 m to elaborate a link window for VLC transmission evaluation.

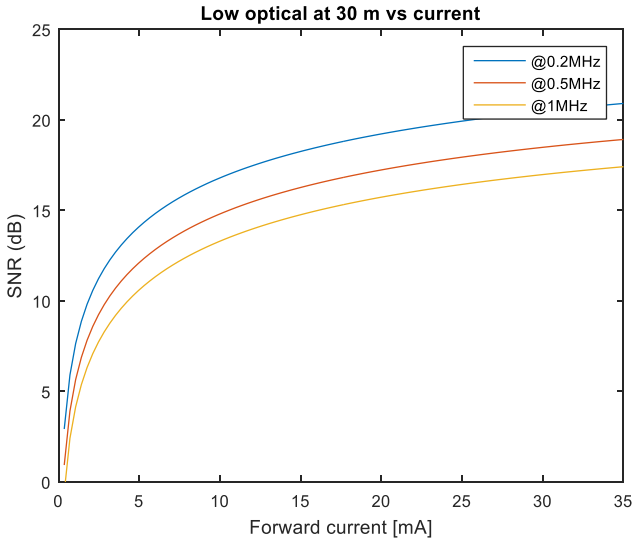

Figure 4.2 SNR vs LED forward current

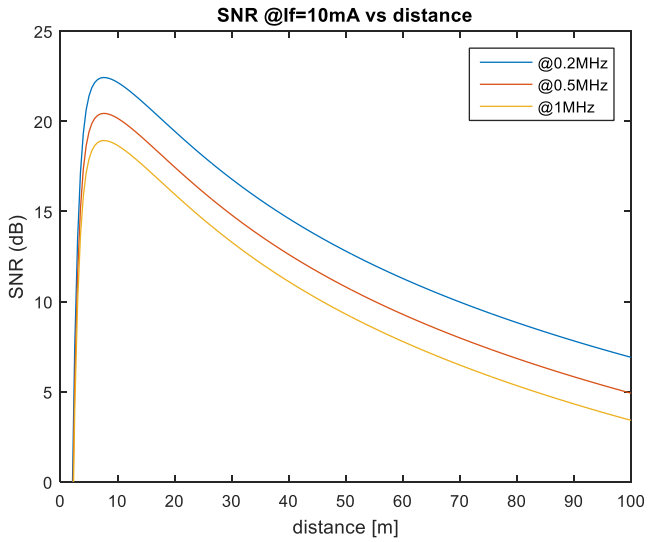

Figure 4.3 SNR with varying horizontal distance

The figures above show the signal to noise ratio, with different bandwidths that vary from 200 kHz to 1 MHz, in this scenario the signal power is always greater than the noise generated at the photo receiver, as it would be expected the signal power decreases with the horizontal distance from the traffic light.

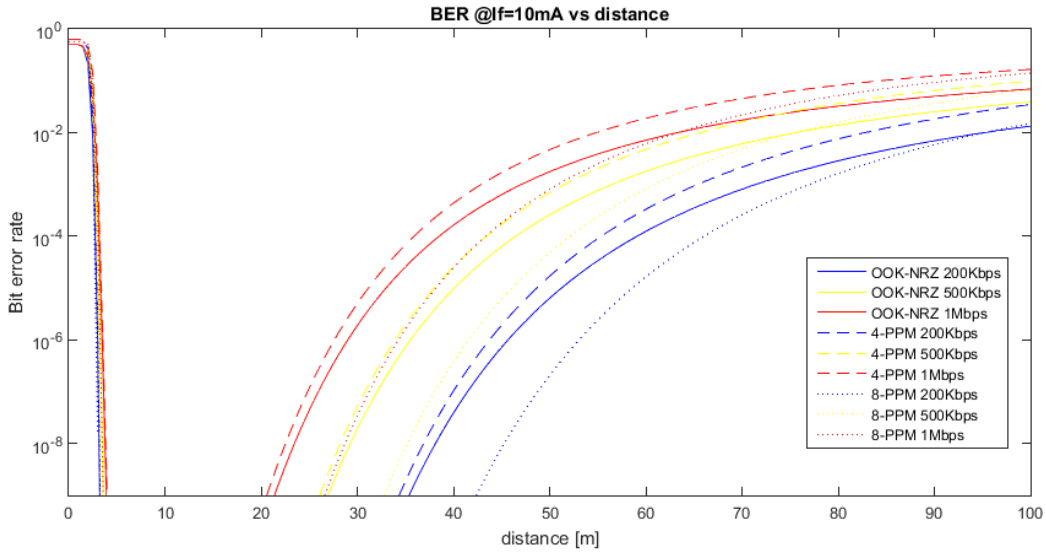

Figure 4.4 bit-error-rate performance for different modulation schemes over horizontal distance

Fig. 4.4 shows the bit-error rate performance for OOK-NRZ at different bit rates and L-PPM with different symbol length, L. The worst performance results come from the 4-PPM at 1Mbps, where at the same data rate, the OOK-NRZ shows similar results. The best performance comes from 8-PPM, reaching a benchmark value of 10^{-6} bit error only at 55 m from the start of the evaluation length, and the high bandwidth requirement of PPM can be acceptable for low data rates.

4.2.2 Artificial light

The light from artificial light sources is almost a certainty in an urban scenario, which is more of a predictable environment for the location of signal traffic lights and the I2C scenario. This optical background interference scenario is more realistic, since numerous street lights are scattered throughout many urban public roads.

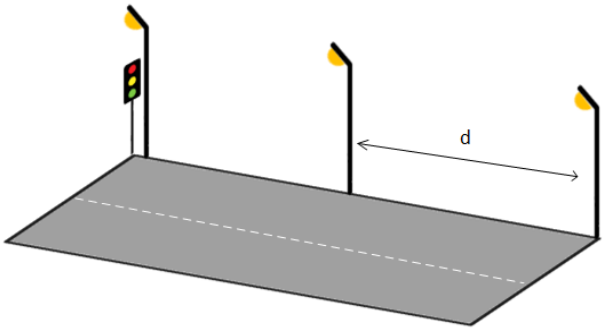

Figure 4.5 Street lamp distribution along the road

In the proposed scenario the street lamp distribution alongside the road length, has a separation distance d=50m and with a mounting height of about 4.5m. The first street lamp is in the vicinity of the traffic light, the second one midway of the road length and the last one at the end of the maximum distance of the simulations. To characterize the optical irradiance power, measurements made with the HD-450 lux meter from Extech, with the photodetector under the street light positioned in an upwards direction at sensibly 1m height. Several measurements were made, covering an array of points under the main radial light intensity.

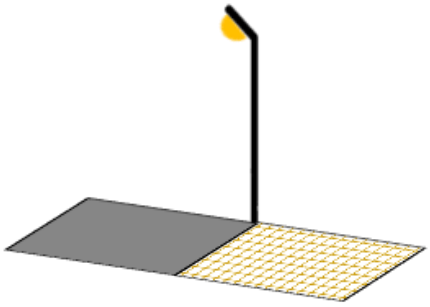

Figure 4.6 Measurement setup grid

The measurements were made over a square grid with 9x9 points and a step of 0.5 m between readings, this resulted in the table located in appendix A. The illuminance peak was measured under the focal point of the radial illuminance pattern of the street light. Considering the full radial pattern of illumination, the recordings obtained only represented a quarter of the total illuminance pattern. To obtain the incident illuminance on the road area, it was created a mirror image of the first measurements matrix to represent the other quarter of radial illumination over the road.

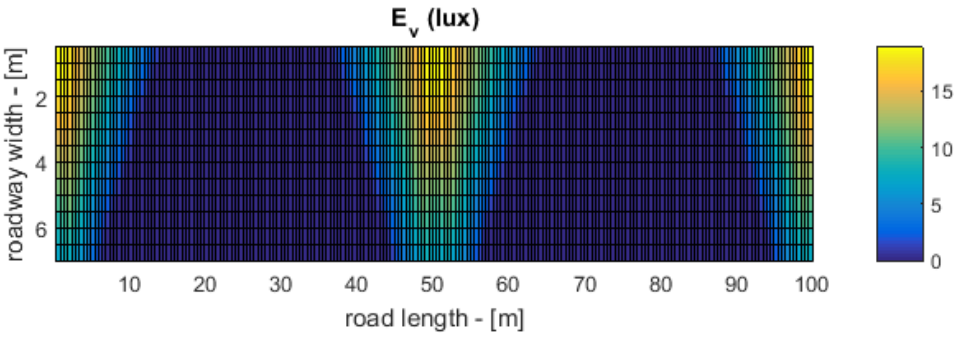

Figure 4.7 Street lamps illuminance (lux) over the road

Fig. 4.7, represents the replication of the illuminance pattern for multiple street lamps with illuminance over the area under simulation.

The measured values were fitted with a curve approximation using MATLAB's curve fitting toolbox, using the least square error approximation. The surface obtained is more homogenous and the area of effect has a broader distribution of illuminance over the entire road under scope. So the illuminance can be a factor of an approximation function $E_v(xi,yi)$, with xi and yi, the receiver Cartesian coordinates on the observation plane. Modelling the incandescent lights with the black body radiation, the irradiance can be given by:

$$E_{inc}(\lambda) = S_p \frac{W(\lambda,2900)}{\max[W(\lambda,2900)]} \quad (4.7)$$

With the peak of spectral irradiance, S_p, obtained similarly as the method developed in the moon's optical irradiance modelling.

$$S_p(xi,yi) = \frac{E_v(xi,yi)}{K_m \int_{\lambda 1}^{\lambda 2} E_0(\lambda) V(\lambda) d\lambda} \quad (4.8)$$

The DC optical background generated photocurrent can be obtained by integrating the spectral power distribution with the detector spectral responsivity:

$$I_{Bg}(xi,yi) = A_d \int_{\lambda i}^{\lambda f} E_{inc}(\lambda,xi,yi)\, \mathcal{R}(\lambda) d\lambda \quad (4.9)$$

Where the total generated photocurrent,

$$I_b = I_{DCsig} + I_{Bg} + I_{dark} \quad (4.10)$$

Which results in a position dependable optical source of noise as a discrete non-uniform interference, with a define area of influence on the evaluated area, depending on the receiver position and FOV.

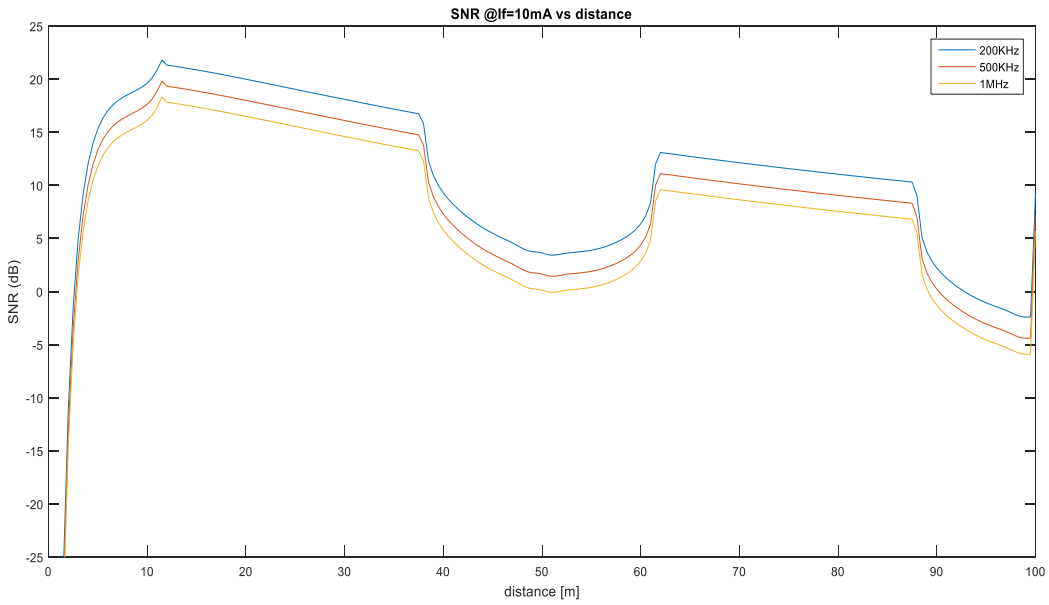

Figure 4.8 Signal-to-noise ratio along the road for different bandwidths, with artificial light interference

Analysing the results in the figure above, it shows how much each street lamps affects the received signal. The first street lamp does not have much impact on the signal to noise ratio, especially due to the incident optical signal from the traffic light is out of the range of the receiver FOV, but under the second and third lamp there is a high increase in noise generated and the signal is not so easy perceivable at the photodetector.

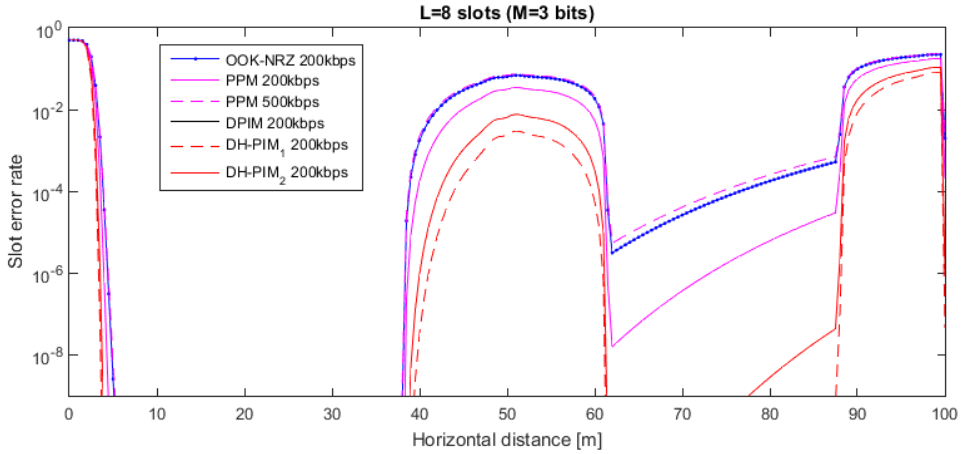

Figure 4.9 Slot error rate for DH-PIM$_{1,2}$, DPIM, PPM and OOK-NRZ

Fig. 4.9, represents the probability of error detection for different modulation schemes. Under irradiance of the street illumination the DH-PIM$_1$, represents the best performance for the asynchronous modulations group.

4.2.3 High intensity natural light

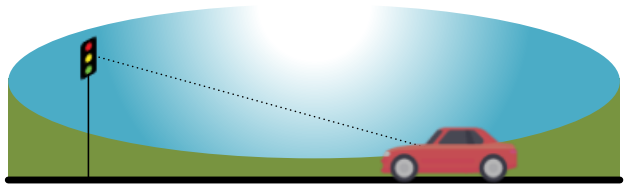

Figure 4.10 Daytime high irradiance scenario on I2C VLC link

The background solar radiation on outdoor VLC systems is one of the greatest challenges in terms of noise presence. Photodiodes directly exposed to sunlight, in the right conditions (clear sky, solar altitude angle and sun's direction) may even get saturated, leading to the inability of detection of the optical signal [32]. Even if the saturation does not occur, the incident solar radiation is a

dominant noise source that greatly limits the communication link performance. Therefore, characterization of the background solar radiation is a major factor when designing an outdoor system.

Predicting the solar radiation is no easy task, creating a model for the background solar radiation at Earth's surface can vary with many different factors, such as: atmospheric effects, including absorption and scattering (Rayleigh) [33]; variations on the local atmosphere, such as water vapour, clouds and pollution; latitude of the location, day of the year and time of day. There is an immense number of variables to consider and no simple way to model all of them with the resources available, especially the diffuse solar radiation from the Earth's atmosphere.

Table 4-2 Measured Solar illuminance at ground level

Measured Solar Illuminance @ Earth's surface	
time	E_v [lux]
12h	147k
12.5h	155.8k
13.5h	146.8k
15h	135k
16h	101k

The illuminance measurements on table 4-2, were made with a lux meter (HD-450 from Extech). These measurements were made during a clear day, with no clouds present and with the lux meter photo sensor pointing at the direction (azimuth angle) of the sun. The elevation angle, α, of the sun at the measured points can be given by [33]:

$$\alpha = \sin^{-1}[\sin(\delta)\sin(\varphi) + \cos(\delta)\cos(\varphi)\cos(HRA)] \quad (4.11)$$

Where, φ is the latitude angle of the location of interest, δ the declination angle and HRA the hour angle. The declination angle represents the Earth's inclination when compared with the Sun's radiation plane and the hour angle converts the number of degrees which the sun moves across the sky [33]. Both the declination angle and the HRA can be given by:

$$\delta = -23.45^{\circ} \cos\left(\frac{360}{365}(d + 10)\right) \quad (4.12)$$

$$HRA = 15^{\circ}(LT - 12) \quad (4.13)$$

In the declination equation, d is the number of days since the beginning of the year time, this number was calculated based on the number of days corresponding since the beginning of the month March, at which the measurements were made. The factor, LT, represents the local time at which the readings were taken. The direct illuminance reading of 16h represents a vertical inclination angle of the sun at 20 degrees approximately. This value was used to simulate the incident normal irradiance on the perpendicular surface of the photodetector. The receiver vertical inclination plane is approximately perpendicular to the incident solar radiation at the elevation angle and is also considered that the road direction is aligned with the sun's azimuth angle. Making this the ideal conditions for the maximum exposure of the photodiode to sunlight.

The optical background noise presence is considered uniform throughout the service area of the I2C link. The same models are used for the moon's irradiance. The sunlight spectral irradiance (W/m^2.nm), is given by:

$$E_{sun}(\lambda) = S_p \frac{W(\lambda,5780)}{\max[W(\lambda,5780)]} \quad (4.14)$$

The spectral radiance pattern is modelled by the black body radiation equation at approximately 5780 Kelvin. With S_p obtained from the photometric to radiometric conversion as in equation 4.2. Where the background illuminance generated photocurrent is given by:

$$I_{sun} = A_d \int_{\lambda i}^{\lambda f} E_{sun}(\lambda)\, \mathcal{R}(\lambda) d\lambda \quad (4.15)$$

Where the DC generated photocurrent is modelled with:

$$I_b = I_{sun} + I_{DCsig} \quad (4.16)$$

The dark current was not included due to its effect being negligible in high optical radiance scenario.

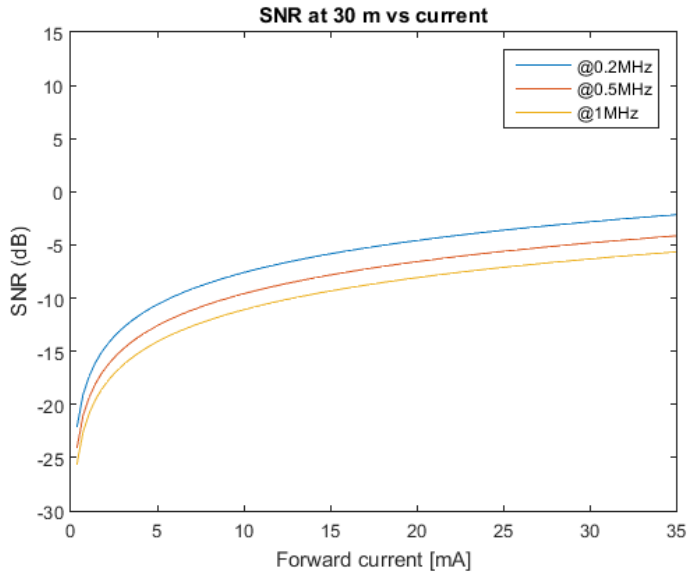

Figure 4.11 Signal to noise ratio vs LED forward current.

The intense optical radiation on the PD, causes a major decline in the signal to noise ratio. Increasing the driving current and consequently the transmitted optical power is very low regarding the noise level.

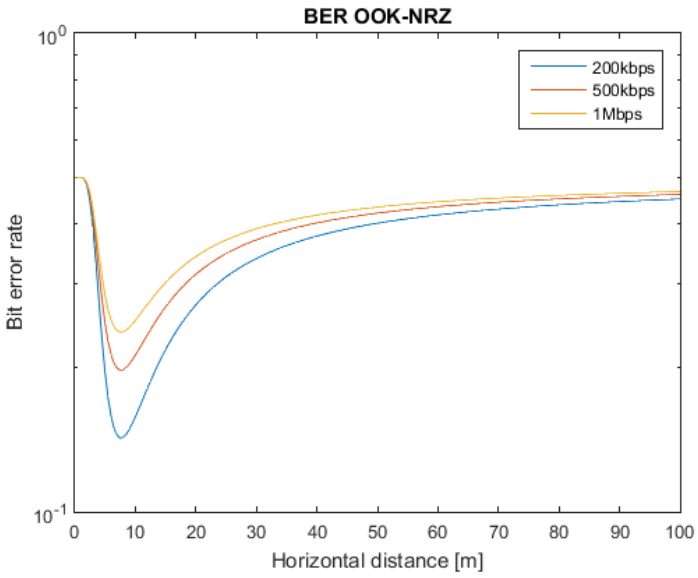

Figure 4.12 BER for OOK-NRZ modulation with different data rates

With direct exposure on the photodetector it is difficult to implement a free error communication, as shown in the figure above an incident optical power so high effects the correct detection of the optical signal. A bit error rate at the receiver lower than 10% points to the necessity of error correcting codes.

4.3 Noise Reduction

Due to the overall white Gaussian noise presence over the spectrum, there are no great possibilities for electronic immunity or reduction under constant optical ambient noise, while applying band-pass electronical filter. It can then be considered the use of external optical elements to produce better signal to noise results. With the optical signal propagating majorly in the red wavelength, but all the visible spectrum may be important regarding other signal sources, like green and yellow signal traffic lights. It is necessary when employing the use of optical filters to maintain a high transmittance rate in the visible range and cutting-off the unnecessary infrared component incident on the PD. Improving signal reception under direct sunlight using an optical filter, although it reduces optical irradiance power from near IR spectrum sources, it also reduces the incident input signal and so there is a trade-off not linearly benefiting the signal-to-noise ratio.

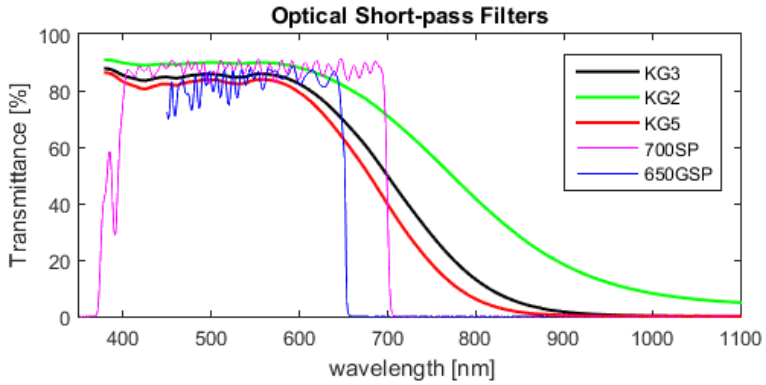

Figure 4.13 Optical Short-pass Filters Transmittance

Fig. 4.13 shows several optical Short-pass filters transmittance rate per wavelength. The slow cut-off filters are from Schott and the fast cut-off filters from Omega Optical.

Table 4-3 Optical short-pass filters price comparison table

MODEL	MANUFACTURER	CUTT-OFF WAVELENGTH	GAIN/LOSS
650GSP	Omega Optical	650 nm	-7.5 dB
700SP	Omega Optical	700 nm	1.4 dB
KG3	Schott	700 nm	0.65 dB
KG2	Schott	800 nm	0.52 dB
KG5	Schott	680 nm	0.6 dB

In SNR simulations several optical filters transmittance function, Tr(λ), were included to filter out as much as possible the non-visible spectral radiation from all optical sources (optical signal also included). In table 4-3, it shows technical characteristics of the employed optical filters as well as the gain/loss results of the filters application in the simulated scenario versus the simulation without optical filter. The 650GSP from Omega Optical even decrease the SNR performance ratings, where the cut-off region was near the optical signal spectral width (optical signal peak at 626 nm).

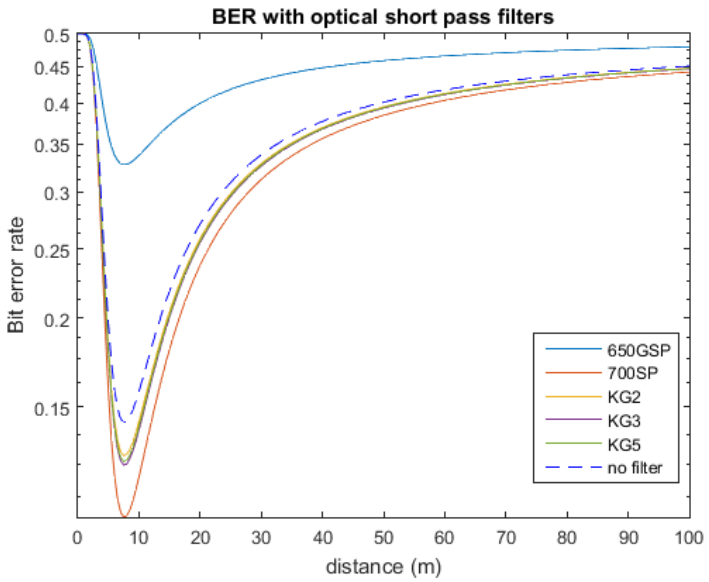

Figure 4.14 bit error rate comparison with different optical filters, with PD exposed to high optical solar radiation

Fig. 4.14 shows the BER performance evaluation for the different band-pass filters under observation, with the receiver noise bandwidth observation range in the 200KHz. The figure above shows the BER improvement for some optical filters, where the best-case scenario comes from the 700SP optical short-pass filter. This filter provides a performance gain of 1.4dB to the signal-to noise ratio but adding this component to the system will incur in a considerable extra cost for the receiver front-end.

5. Chapter 5

5.1 C2C Communication link

The car-to-car communications link physical layer is supported by a VLC channel, connecting car headlamps as emitters to a receiver on the back-end of a second car. The inverse could also be a possible, using break lights or other kind of signalling car lights. This communication link can have many applications in ADAS (advanced driver-assistance systems) providing useful information of driving conditions to the human user in order to mitigate human error and promote a safe driving environment, for example proximity sensing and sending warning messages to both the involved drivers.

This chapter will discuss the C2C communication link, describing the emitter model for a car headlamp, examining the radiation pattern, describing the channel model for the first order reflection and an adapted version for direct line of sight signal propagation. The effects of multipath propagation are taken into consideration for this simulation and are evaluated by the channel impulse response and the delay spread. Finally, modulation schemes simulation performance of the C2C communication link.

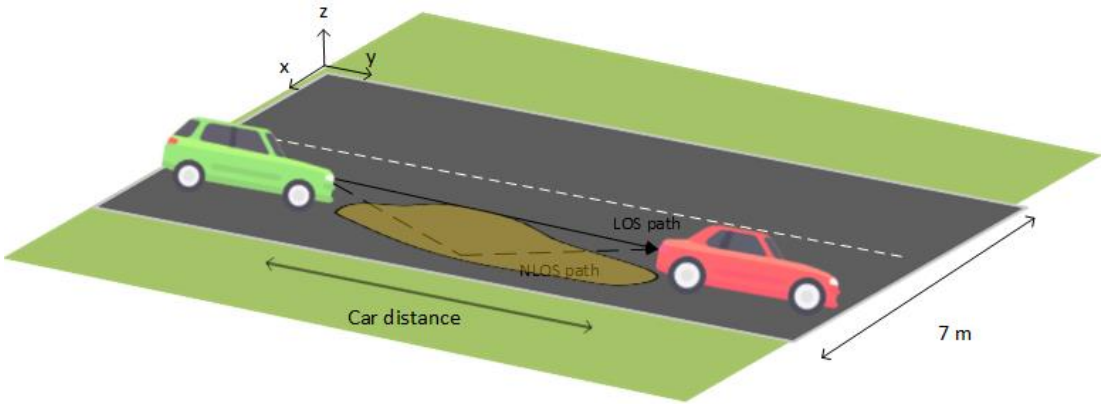

Figure 5.1 C2C scenario

A typical C2C scenario is represented in fig. 5.1, with LOS and non-LOS optical path propagation. The simulation parameters included for a mathematical model of C2C communication link include:

- Car headlamp optical beam pattern
- Road surface reflection (first reflection model)
- Noise sources spectral power, including natural and artificial lights (from I2C simulations)
- Characterization of the White LED spectrum
- Receiver spectral response (from I2C simulations)

5.2 Emitter model

Automotive front lighting evolution has been focused on achieving optimal illumination of the near road space in front of the driver, with the objective of road illumination and its surroundings as much as possible so that the driver is able to identify obstacles on its path. In another regard they should protect preceding pedestrians or oncoming drivers from excessive glare. So vehicular lighting technology while being developed to provide drivers more illumination of oncoming road path, having higher visibility can result in higher glare for to other drivers travelling in an opposite direction, causing glare and detrimental visibility to them. Typically, the use of low beams in high traffic areas is a more common and advised solution. Low beams provide a light distribution that provides enough lateral and forward road illumination without interfering with other drivers. Performance specification for headlamps light distribution indicating the maximum output and beam patterns (with intensity distribution on variable angle of emission), have been established by regulatory bodies [34].

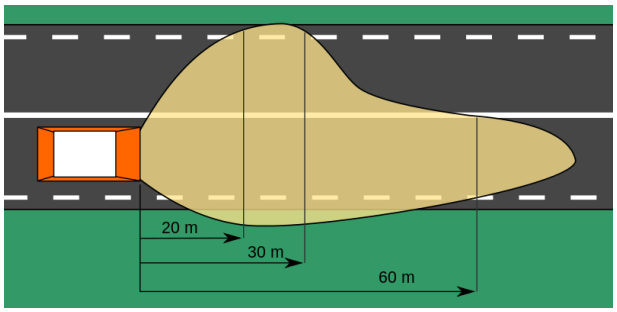

Figure 5.2 Illustration showing the right-hand traffic, asymmetrical low beam pattern characterized by an extended visual range along the right side lane of the road [34]

Fig. 5.2 shows the low beam projection pattern that provides adequate forward and lateral illumination, with controlled glare directed to oncoming drivers.

New technologies have been employed along the year when developing new car headlamps, in the early seventy's halogen bulbs replaced incandescent bulbs and increased the amount of light output. In the early nineties high intensity discharge (HID) lamps were developed for vehicles, these lamps had a higher luminous efficacy, and a longer life than conventional systems. Vehicular visible light communication would require the utilization of an automobile LED headlamp as an emitter, as LED vehicle headlamp lighting systems are a natural progression in this line. The development of white LED technology with increased lumen output per device has increased manufacture's intention on implementing LED technology in the development of optical vehicle components [35]. White LED efficiency of commercial use has reached values around 150 lm/W [36]. A white LED spectral power distribution tries to emulate a spread distribution over the visible range, but current LEDs on the market show a specific distribution with different wavelength peaks, as shows fig 5.3.

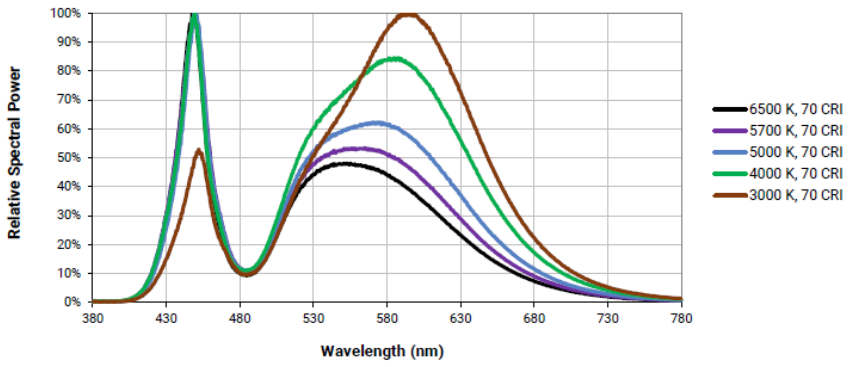

Figure 5.3 Relative spectral power distribution of a White LED lamp (CMT1922, from Cree)

Creating a model for a car headlamp for VLC communication cannot be described by a LED Lambertian radiation pattern, as it has an asymmetric radiation pattern. The emitter optical propagation is described by a market weighted study [37] for headlamps intensity output, and thus having a more realistic optical propagation model for a low beam headlamp as a VLC emitter.

5.2.1 Radiation pattern

Low beams, or dipped beam, provide an asymmetrical illumination pattern that ensures enough lateral and forward illumination without inducing glare in opposing drivers or other pedestrians. The data obtained from a market-weighted headlamp beam pattern study [37] was used in the C2C simulations to reproduce a car headlamp emitting pattern, these values are present on a table in appendix A. It was necessary to have a fitting model for integrating the empirical data in a simulation context. Using the curve fitting tool from MATLAB, the LOWESS (locally weighted smoothing surface) method was used to approximate the luminous intensity surface vs horizontal and vertical angle. This method, LOWESS, has a big disadvantage is that it does not produce a regression function, making it difficult to transfer the results to other people [38]. The LOWESS method only requires a smoothing parameter and the degree of the local polynomial function (quadratic) which approximates local subsets of data. This model achieved a goodness of fit specified by R^2=0.9964.

The modelled isocandela illuminance diagram in MATLAB produced an isocandela function for a headlamp emitter, that is described by a fit of luminous intensity I(α,β) from the obtained data, being α and β, the vertical and horizontal angles (according to the headlamp axis). In the figure below is the distribution for a low beam headlight lamp, based on the market-weighted headlamp beam pattern, with LOWESS fit [37].

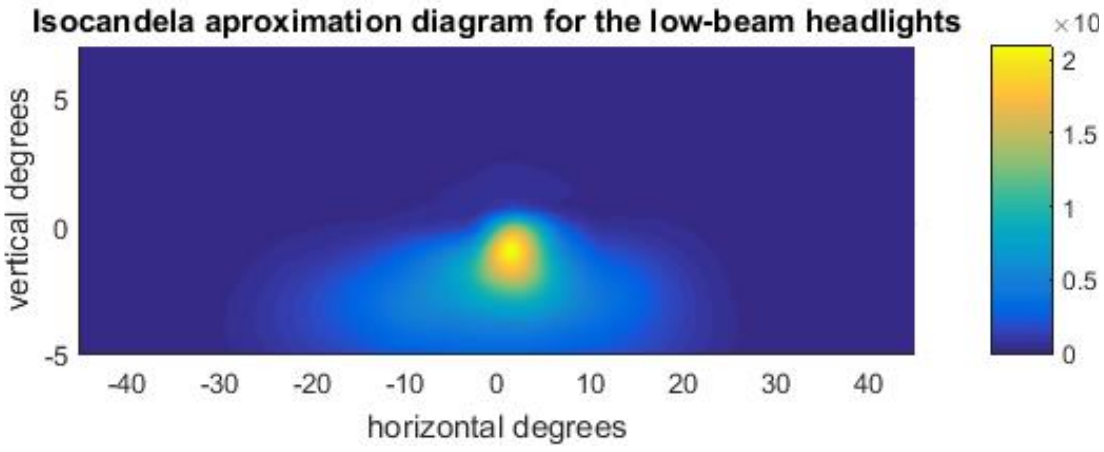

Figure 5.4 Radiant diagram for headlamp light distribution

The illuminance, E, incident on a surface with angle of incidence , ψ, from a car headlamp luminous intensity radiation pattern can be obtained by [1]:

$$E = \frac{d\phi_v}{dS} = \frac{I(\alpha,\beta)}{d^2}\cos(\psi) \quad (5.1)$$

Where $d\phi_v$ is the luminous flux (lumens), S the area of the surface (m^2), I(α,β) is the luminous intensity (cd), α and β, the vertical and horizontal angles respectively, d the distance between emitting light and receiver surface. Being the distance, $\vec{d}$, given by:

$$\vec{d} = (x - x_E, y, z - z_E) \quad (5.2)$$

Considering both headlamps of the emitting car with are located at Tx1= (4.65, 0, 0.5) and Tx2= (5.85, 0, 0.5), z_E representing the headlamps height and x_E being the lateral distance position of each headlamp. The total illuminance can be given by:

$$E_{total} = E_{Tx1} + E_{Tx2} \quad (5.3)$$

Where each emitting headlamp,

$$E_{Tx} = \frac{I(\alpha,\beta)}{[(x-x_E)^2+y^2+(z-z_E)^2]^2}\cos(\psi) \quad (5.4)$$

The horizontal and vertical angles can be given by:

$$\beta = \tan^{-1}\left(\frac{x-x_E}{y}\right) \quad (5.5)$$

$$\alpha = \tan^{-1}\left(\frac{z-z_E}{y}\right) \quad (5.6)$$

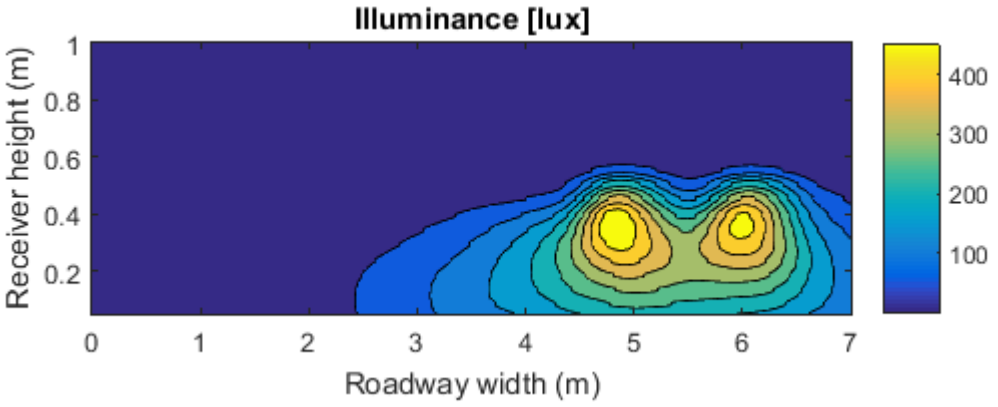

Figure 5.5 Illuminance on a vertical plane, at 7 m distance

Fig. 5.5 represents a vertical plane illuminance (lux) distribution from the two car headlamps, with a longitudinal distance (y- axis) of 7 m to the receiver plane. The combination from both headlamps provides a more uniform illuminance scenario.

5.3 LOS and NLOS propagation

The predecessor simulations presented in this dissertation were based on LOS path propagation, but in the present scenario as the typical emitter/receiver location are nearer of the road surface, the reflections induced by this surface can become a more influential factor, when describing the VLC C2C channel. Other surfaces in the nearby vicinity could also be an influential, such as buildings and/or houses in narrow streets, but as the only guaranteed surface that can be taken into consideration is the road. In the proposed scenario optical signal propagation occurs directly with the light following a LOS path or indirectly reaching the PD through reflections on nearby surfaces.

Modelling the LOS path loss component from one headlamp can be extrapolated from the model equations in chapter 2, but instead of using the Lambertian emitting pattern typical from LEDs, for the headlamp radiation model is required to use a different kind of optical intensity radiation pattern. Which can be described with the isocandela radiation pattern typical for car headlights. The LOS optical propagation equation takes the form of the equation below.

$$P_{LOS} = \frac{I(\alpha,\beta)A_r \cos\psi}{d^2} rect\left(\frac{\psi}{FOV}\right) \quad (5.7)$$

5.3.1 Platform illustration

The simulated C2C VLC communication scenario implies the location of two cars on the right-side lane of a road, with a variable mean car distance d and a total road width of 7 meters. The emitter/receiver pair is located at 0.5m distance of the road surface, with the receiver orientation towards the car opposing direction and the emitters signal propagation dependent on the headlamp light distribution.

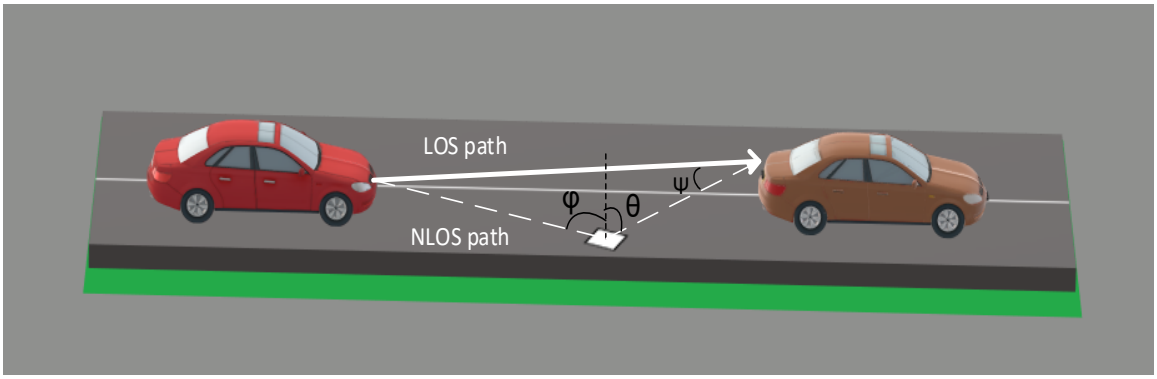

Figure 5.6 C2C communication link with direct path and diffuse reflected path

The schematic diagram of the C2C VLC system is illustrated in figure 5.6. Note that the receiver (Rx) captures optical power from both right (rsh) and left (lsh) headlamps and only rays coming from the right headlamp are illustrated. Being the received power given by [36]:

$$P_{rx} = Plsh_{LOS} + Prsh_{LOS} + Plsh_{NLOS} + Prsh_{NLOS} \quad (5.8)$$

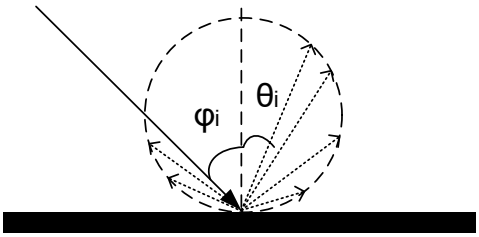

Figure 5.7 Diffuse Lambertian reflection on the road surface for an area element

The reflection on the road surface is modelled with a Lambertian profile of the reflected light, the road surface was divided into multiple area elements (dA). The reflection contribution of the road can be computed with the given model:

$$R(\varphi) = \frac{\rho \cos(\varphi)\cos(\theta)dA}{\pi} \quad (5.9)$$

Where ρ is the road reflection coefficient, φ the incident light beam angle and θ the reflected light beam output angle. A single incident optical beam propagates into multiple paths generating multiple reflection originated from a single element area surface.

The path loss of a reflection, diffuse optical power propagation, for the right-side lamp can be approximated by:

$$NLOS_{rsh} = \frac{I_R(\alpha,\beta)A_r \cos(\varphi)\cos(\theta)\cos(\psi)\rho dA}{(d_T^2+d_R^2)\pi} rect\left(\frac{\psi}{FOV}\right) \quad (5.10)$$

But with multiple reflections elements of the surface area, the above equation develops into:

$$Prsh_{NLOS} = \sum_{n=1}^{N_{pts}} \frac{I_R(\alpha_n,\beta_n)A_r \cos(\varphi_n)\cos(\theta_n)\cos(\psi_n)\rho dA}{(d_{Tn}^2+d_{Rn}^2)\pi} rect\left(\frac{\psi_n}{FOV}\right) \quad (5.11)$$

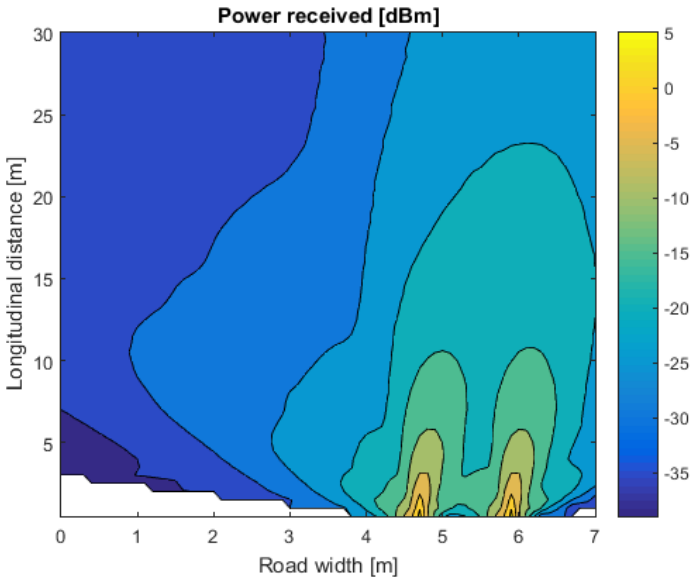

Figure 5.8 Average received power over the roadway service area

Figure 5.8 depicts the incident optical power on the receiver, with variable position along the road width with longitudinal distance up to 30m. Standard receiver height at 0.5 m. It shows the tendency of most of the radiation pattern tends to the right and its non-symmetry along the right-side car lane. The emitting car centre location is at 5.25m from the edge of the road, which locates him in the mean centre position of the right-side lane of the roadway.

5.4 Multipath Propagation

Multipath propagation induces limitations on the VLC link, while inducing inter symbol interference (ISI) due to the multiple paths' optical propagation for the data to travel to the receiver. With high enough delayed components reaching the PD, interfering with the detection of the pulse at a given sampling time.

5.4.1 Channel impulse response

The CIR (channel impulse response) component due to each headlamp can be modelled as a combination of attenuation values and time delays regarding the emitted optical pulse. Thus accounting for all the reflective components that contribute with incident power on the PD, it is constructed the CIR response vector with each component located in the correct time travel span, obtained from the total distance (d_{Tn}+d_{Rn}) travelled by the reflected optical components [39].

$$h(t) = \sum_{n=1}^{N_{pts}} P_n \delta\left(t - \frac{(d_{Tn}+d_{Rn})}{c}\right) \quad (5.12)$$

Where P_n is the power component corresponding to indirect optical propagation from the first reflection of the road bounce model, relative to an area element of reflection. The number of area elements for optical reflection is totalized by N_{pts}, by equally dividing the reflection road surface into dA elements. The reflection ray travel time is estimated with the total reflection propagation

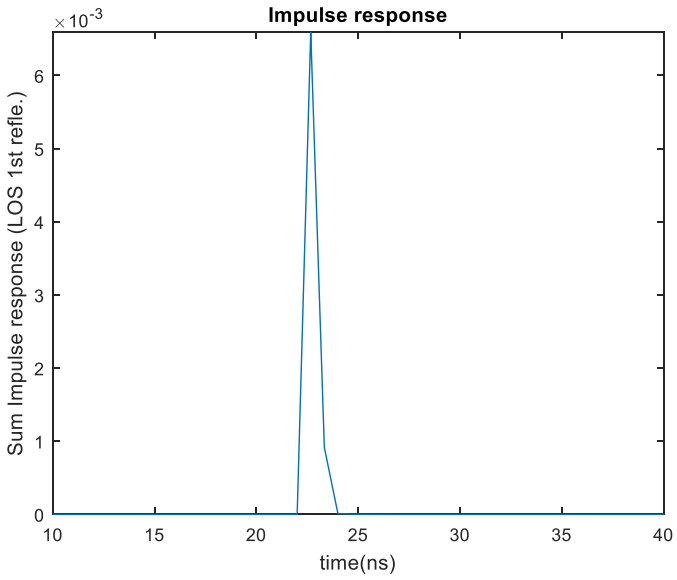

Figure 5.9 Channel impulse response example

distance and the speed of light constant and the time resolution of the CIR vector is around 0.66 ns.

The figure above represents the line of sight and first reflection channel impulse response with a car separation of 7 meters and an alignment offset of 1 meter.

5.4.2 Delay Spread

The temporal spread response can be defined by the root mean square delay spread (D_{rms}), which defines the physical channel upper bandwidth limitation. An accurate model of all channel reflection elements would provide a more comfortable measure for this parameter and thus the real particularities of different scenario locations of a C2C scenario, but with never-ending changes of different vehicles in the road and different weather conditions, the resume of reflective surfaces on the VLC channel rest on the road surface and its effects on an information pulse temporal spread.

The delay profile is composed of the two headlights line of sight links (LOS components) and a greater number of non-lines of sight (NLOS) delay taps. The temporal dispersion of the power delay profile can be expressed by the excess delay (μ) and the channel root mean square (RMS) delay spread (D_{rms}), these parameters are given by [40],

$$\mu = \frac{\sum_{i=1}^{2} P_{los.i}.t_{d,i} + \sum_{j=1}^{N} P_{nlos,j}.t_{ref,j}}{P_{rx}} \quad (5.13)$$

$$\mu^2 = \frac{\sum_{i=1}^{2} P_{los.i}.{t_{d,i}}^2 + \sum_{j=1}^{N} P_{nlos,j}.{t_{ref,j}}^2}{P_{rx}} \quad (5.14)$$

With t_d being the direct path travel time and t_{ref} the actual main impulse delay power from the reflection on the road surface. The delay square root mean square being:

$$D_{rms} = \sqrt{\mu^2 - (\mu)^2} \quad (5.15)$$

Where P_{rx} is the total received power from equation 5.8. The simulation results are displayed in the fig. below, the display over the communication channel area, with width of the road right side lane (3.5 meters) and variable car distance up to 30 m. The delay spread simulation takes into consideration an alignment between cars and due to the headlight's intensity, the central area of communication does not appear to have too much delay spread. In the figure below, it shows the simulation results for the delay spread (RMS) from the receiver car point of view, with the increasing distance between cars the reflecting road surface was incremented to match the available reflection plane.

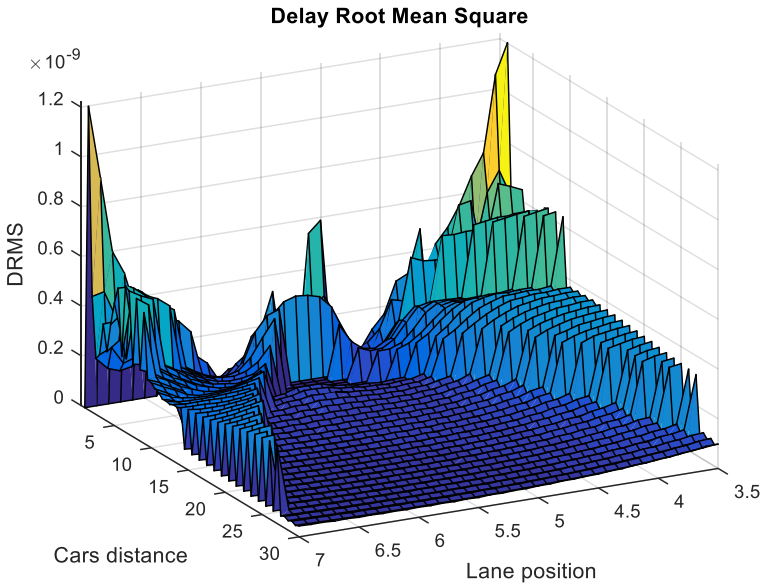

Figure 5.10 DRMS – of the service area; link connection between cars

The simulations results show that after 30m distance between vehicles and over the right-side lane width, the relative misalignments between vehicles inside the same lane would have minimized delay spread effects, along these long distances the LOS component over the roadway width is much superior than the diffuse component.

The channel bandwidth limitations from the RMS delay spread, D_{rms}, impose a limit on the transmission rate R_b, which can be given by [1]:

$$R_b \leq \frac{1}{10D_{RMS}} \qquad (5.16)$$

The root mean delay spread of this setup under consideration is around 1.4 ns, with the receiver location near the extremities of the road lane. Hence the maximum achievable data rates are limited to up to 70 Mbps, considering the free mobility between vehicles and this number can decrease for wider road lanes.

5.5 C2C Modulations Performance

In this final subchapter it will present the performance evaluation of the proposed baseband modulations schemes in the C2C scenario. Different optical background irradiance sources are simulated similarly to the I2C scenario. The error performance on the considered AWGN with predominant shot-noise, is modelled with the signal to noise ratio observed at the receiver, given by:

$$\frac{E_b}{N_o} = \frac{(mP_{rx}\mathcal{R})^2}{\sigma_{shot}^2}$$

Where P_{rx} is the average optical power received in Watts with a white LED optical power distribution, $\mathcal{R}$ the photodetector responsivity and the shot-noise variance,

$$\sigma_{shot}^2 = 2qI_{DC}BW$$

With q is the electron charge, $I_{DC}=I_{DCsig}+I_{Bg}$ the generated DC photocurrent at the receiver from the headlamps and optical background irradiance. The observable bandwidth is represented by BW.

The simulations results presented were a result of LOS and non-LOS optical signal propagation due to the data throughput proposed produces a bandwidth occupancy at maximum of a few MHz. Therefore, the multipath induce ISI can be considered negligible. It is also considered that the centreline of the emitting car is aligned with the receiver at the second car and a simulated maximum car distance of 30m.

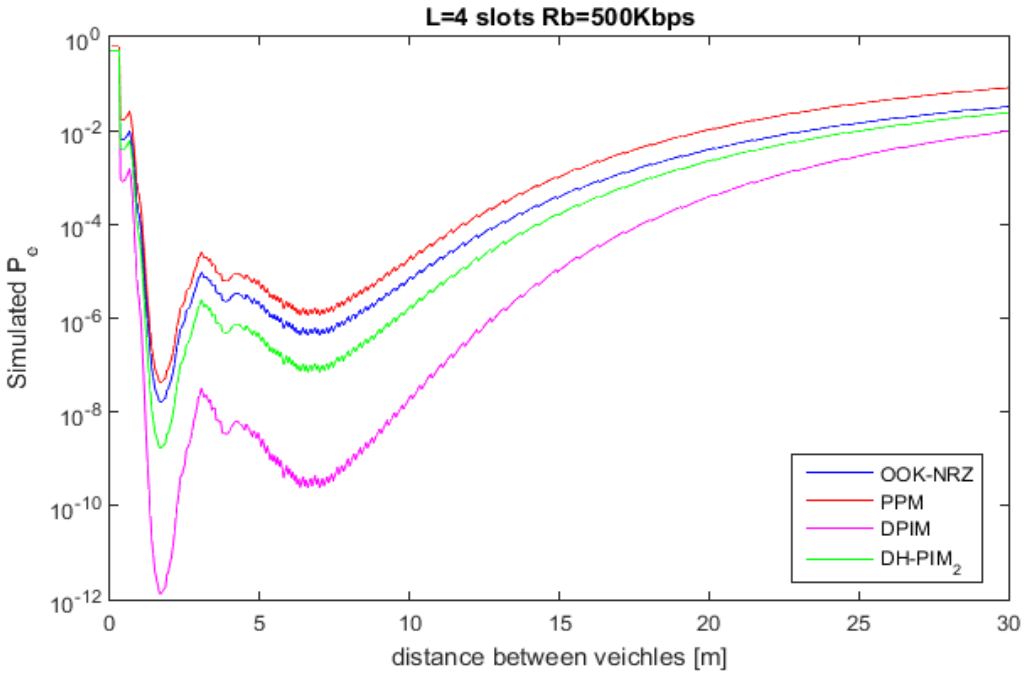

Figure 5.11 Slot error rate for DH-PIM2 and DPIM, compared to bit error rate of PPM and OOK. Under moon optical background irradiance.

Fig 5.11 shows baseband modulations performance under low optical background illuminance from the moon. In this idealist scenario the communication range can easily reach 10-15 m between vehicles without the need for any accommodation or error correcting techniques, at a data rate of 500Kbps. DPIM modulation scheme shows the best error performance, but when comparing its behaviour to the OOK-NRZ or PPM, where pulse detection error is confined to a symbol, it is necessary to account for the possibility of DPIM nearby symbols also having an incorrect interpretation.

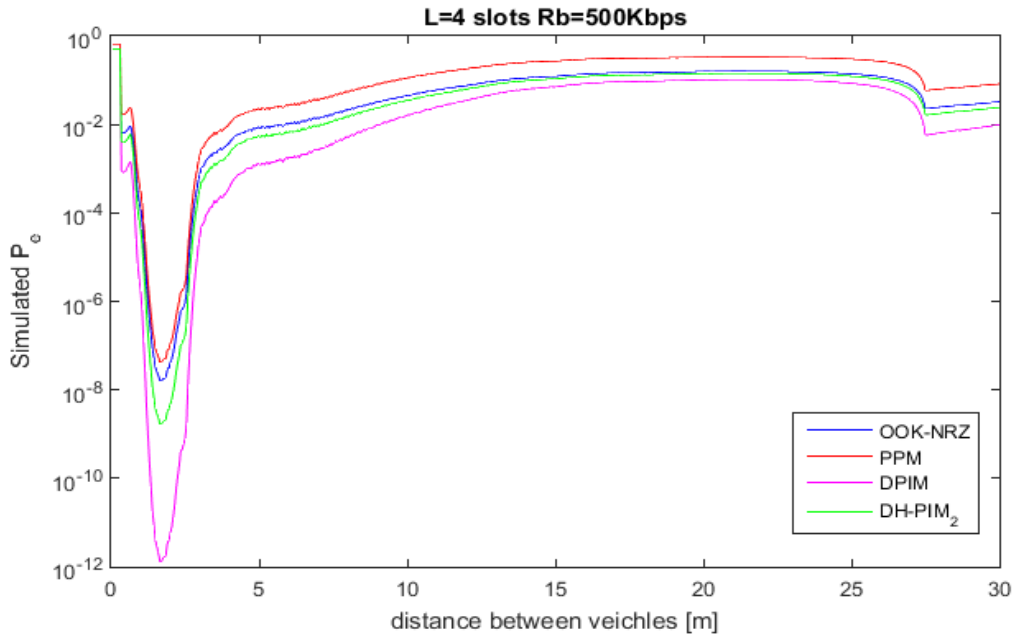

Figure 5.12 Slot error rate for DH-PIM2 and DPIM, compared to bit error rate of PPM and OOK. Under street lamp illuminance.

Fig. 5.12 shows the performance of the I2C scenario under a street light optical background irradiance located at the middle of the evaluation distance. Under high artificial optical irradiance, from the street light, the performance levels for all modulation schemes require error correcting codes for a viable communication link, at almost all the evaluated distance. PPM spectral distribution has the lowest DC component from the proposed schemes and this can be an ideal modulation scheme under artificial lights, for immunization against AC sinusoidal interference produced.

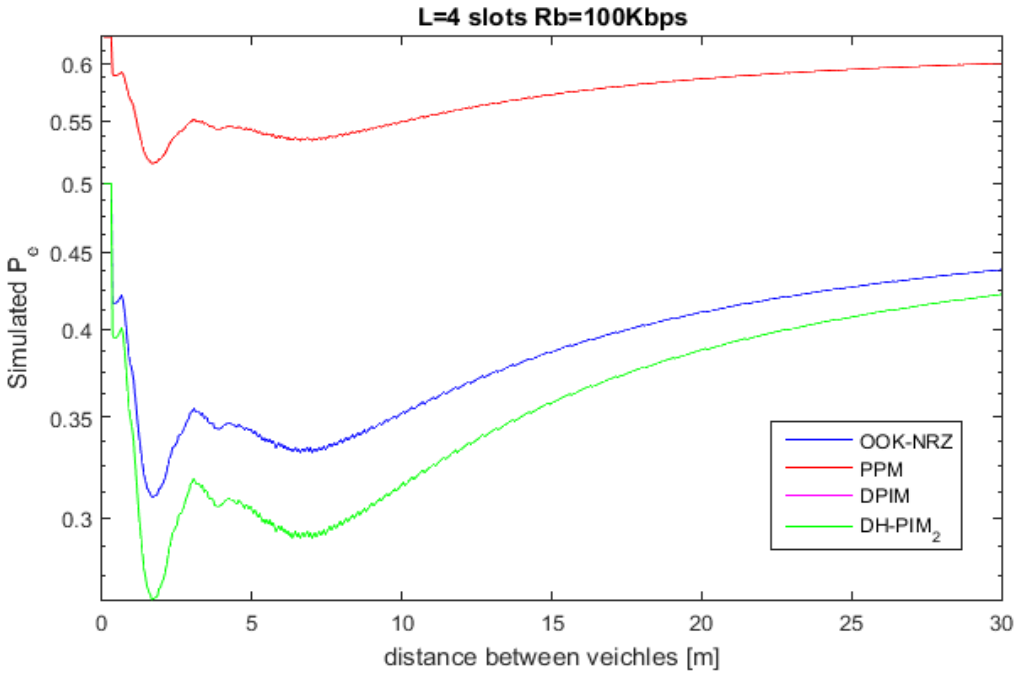

Figure 5.13 Slot error rate for DH-PIM2 and DPIM, compared to bit error rate of PPM and OOK. Under solar background irradiance.

Fig. 5.13 shows the predicted performance for OOK-NRZ, PPM, DPIM and DH-PIM$_2$ modulations schemes with the same symbol length, L=4, and a data rate of 100Kbps. The high optical irradiance reaching the photodetector induces a low performance for all modulation schemes with a high error rate. Making this the worst-case scenario for outdoor communications systems, where the necessity for direct solar irradiance immunity must be taken as a great challenge. A photoreceiver with stimulation only by high frequency optical signals would be a great achievement for VLC.

6. Chapter 6

6.1 Conclusion

The main goal of this work was to observe and simulate the behaviour of outdoor VLC communication systems under different optical scenarios. The models for direct optical path propagation are based on studies referenced on chapter 2. With this work it was possible to 3D model the optical path propagation in LOS, giving a good description of the received signal power and the DC component from the optical emitter.

The different proposed ambient scenarios provide a reliable view of the achievable data transmission rates under different optical background noise sources. Also, is considered the distance at each scenario the communication can be maintained without the necessity of error correcting codes. In low optical noise scenario, it is possible to maintain a good communication link performance up to 40 m distance between transceivers, with bit-error-rate below the benchmark level of 10^{-6}. In the presence of artificial lights, the performance drops considerably for any baseband modulation simulated. Under high solar irradiance scenarios, the bit-error-rate values usually higher than 10%, which implies the use of error correcting codes to maintain a communication link. The optical filters included in these simulations, produced a very low gain in signal to noise ratio.

The multipath optical propagation in the C2C scenario from road reflections limited the transmission data rate at 70Mbps. When comparing this limitation to a LEDs optical bandwidth in the range of a few MHz's, it proves that the road reflection has a limited impact on data throughput.

6.2 Future work

For possible future work approaches there are several topics that can be developed, such as:

- Full solar irradiance model, based on the channel geographical location, time of the year and receiver orientation vs solar altitude and azimuth angle. Solar irradiance immunity improvements with more expensive narrowband optical pass filters.
- Digital fountains algorithm application in broadcast communication I2C scenario. Study of the optimization of data packet delivery to multiple receivers/clients.
- Implementation of the I2C system transceiver architecture with more viable, low cost and market-oriented resources.

Bibliography

[1] Z. Ghassemlooy, L. A. Nero, S. Zvánovec, and M.-A. Khalighi, *Visible Light Communications Theory and applications*. 2017.

[2] "Understanding Light Spectrum." [Online]. Available: https://eyelighting.com/lighting-technology-education/general-lighting-basics/light-spectrum.

[3] C. Chappe, "Chappe's Telegraph Semaphore." [Online]. Available: https://pt.wikipedia.org/wiki/Claude_Chappe. [Accessed: 11-Sep-2018].

[4] G. Bell, "Photophone." [Online]. Available: https://en.wikipedia.org/wiki/Photophone. [Accessed: 11-Sep-2018].

[5] N. Lourenço, D. Terra, N. Kumar, L. N. Alves, and R. L. Aguiar, "Visible Light Communication System for Outdoor Applications," *Proc. 2012 8th Int. Symp. Commun. Syst. Networks Digit. Signal Process. CSNDSP 2012*, 2012.

[6] N. Kumar, D. Terra, N. Lourenco, L. Nero Alves, and R. L. Aguiar, "Visible light communication for intelligent transportation in road safety applications," *IWCMC 2011 - 7th Int. Wirel. Commun. Mob. Comput. Conf.*, pp. 1513–1518, 2011.

[7] IRTAD, "Road Safety Annual Report 2018," 2018.

[8] World Health Organization, "Global status report on road safety 2015," 2015.

[9] N. Kumar, D. Terra, A. Tavares, and R. L. Aguiar, "VIDAS - D2.1 System conceptual design," Aveiro, 2010.

[10] G. L. Lial, "Controlo de tráfego," Instituto Superior de Engenharia de Lisboa, 2011.

[11] N. Lu, N. Cheng, N. Zhang, X. Shen, and J. W. Mark, "Connected vehicles: Solutions and challenges," *IEEE Internet Things J.*, vol. 1, no. 4, pp. 289–299, 2014.

[12] L. U. Khan, "Visible light communication: Applications, architecture, standardization and research challenges," *Digit. Commun. Networks*, vol. 3, no. 2, pp. 78–88, 2017.

[13] S. Haruyama, "Visible Light Communication," *J. Inst. Image Inf. Telev. Eng.*, vol. 64, no. 9, pp. 1337–1338, 2010.

[14] N. Kumar, N. Lourenço, L. N. Alves, and R. L. Aguiar, "VIDAS D3.1 Channel characterization

of outdoor VLC channel," Aveiro, 2010.

[15] Z. Ghassemlooy, W. Popoola, and S. Rajbhandari, *Optical Wireless Communications: System and Channel Modelling with Matlab®*. 2012.

[16] M. V. Bhalerao, M. Sumathi, and S. S. Sonavane, "Line of sight model for visible light communication using Lambertian radiation pattern of LED," *Int. J. Commun. Syst.*, vol. 30, no. 11, p. e3250, 2017.

[17] E. F. Schubert, *Light-Emitting Diodes Second Edition*, 2nd editio., vol. 39, no. 5. Cambridge University Press, 2008.

[18] Avago Technologies, "HLMP-EGxx Data Sheet." pp. 1–11, 2012.

[19] M. da A. Interna, "Diário da República - Decreto Regulamentar nº22-A/98," *October*, no. 2, 1998.

[20] S. B. Alexander, *Optical Communication Receiver Design*, vol. 37, no. 1. 2007.

[21] B. Sklar, *Digital Communications Fundamentals and Applications 2nd Edition*, 2nd editio., no. 1132. Prentice Hall PTR, 1987.

[22] R. C. of America, *Electro-Optics Handbook: A Compendium of Useful Information and Technical Data*. RCA/Commercial Engineering, 1974.

[23] Wikipedia, "Black body." [Online]. Available: https://en.wikipedia.org/wiki/Black_body. [Accessed: 04-Jul-2017].

[24] A. V. Raisanen and A. Lehto, *Radio Engineering for Wireless Communication and Sensor Applications*. Artech House, Inc.

[25] M. . McCullagh, P. P. Smyth, D. R. Wisely, and P. L. Eardley, "Optical wireless LANs: applications and systems," *IEEE Photonics Webinar*. Institute for Photonic Integration, Eindhoven, p. 8, 2018.

[26] P. Camacho, "Front-End Design for Visible Light Communications Systems," Universidade de Aveiro, 2017.

[27] Luis Filipe Mesquita Nero Moreira Alves, "Estudo e Implementação de Amplificadores em Modo de Corrente com Grande Produto Ganho Largura de Banda Luis Filipe Mesquita Nero Moreira Alves Estudo e Implementação de Amplificadores em Modo de Corrente com Grande Produto Ganho Largura de Banda," Universidade de Aveiro, 2008.

[28] “Digital Communication - Line Codes.” [Online]. Available: https://www.tutorialspoint.com/digital_communication/digital_communication_line_codes.htm.

[29] D. Karunatilaka, F. Zafar, V. Kalavally, and R. Parthiban, “LED Based Indoor Visible Light Communications: State of the Art,” *IEEE Commun. Surv. Tutorials*, vol. 17, no. 3, pp. 1649–1678, 2015.

[30] N. M. Aldibbiat, Z. Ghassemlooy, and R. McLaughlin, “Performance of Dual Header-Pulse Interval Modulation (DH-PIM) for Optical Wireless Communication Systems,” *IEE Proc. - Optoelectron.*, vol. 148, no. 2, pp. 91–96, 2001.

[31] D. Zhang and S. Hranilovic, “Bandlimited Optical Intensity Modulation under Average and Peak Power Constraints,” *IEEE Trans. Commun.*, vol. 64, no. 9, pp. 3820–3830, 2016.

[32] K. Cui, G. Chen, Z. Xu, and R. D. Roberts, “Traffic light to vehicle visible light communication channel characterization,” *Appl. Opt.*, vol. 51, no. 27, pp. 6594–6605, 2012.

[33] C. Honsberg and S. Bowden, “Photovoltaic Education,” 2018. [Online]. Available: https://www.pveducation.org. [Accessed: 18-Oct-2018].

[34] K. Minolta, “Photometric Specification of Automotive Headlamp.”

[35] J. F. Van Derlofske and M. McColgan, “White LED sources for vehicle forward lighting,” *Proc. SPIE*, pp. 195–205, 2002.

[36] P. Luo, Z. Ghassemlooy, H. Le Minh, W. Viriyasitavat, and H.-M. Tsai, “Car-to-Car Visible Light Communications from: Visible Light Communications,Theory and Applications Routledge,” in *Visible Light Communications Theory and Applications*, 2017, pp. 225–252.

[37] M. Sivak, M. J. Flannagan, B. Schoettle, and W. J. Kosmatka, “SAE TECHNICAL A Market-Weighted Description of Low-Beam Headlighting Patterns in the U . S .,” Ann Arbor, Michigan, 2004.

[38] “Local regression,” *Wikipedia*. [Online]. Available: https://en.wikipedia.org/wiki/Local_regression.

[39] J. R. Barry, J. M. Kahn, W. J. Krause, E. A. Lee, and D. G. Messerschmitt, “Simulation of Multipath Impulse Response for Indoor Wireless Optical Channels,” *IEEE J. Sel. Areas Commun.*, vol. 11, no. 3, pp. 367–379, 1993.

[40] S. S. Muhammad, “Delay profiles for indoor diffused visible light communication,” *Proc. 13th*

Int. Conf. Telecommun. ConTEL 2015, no. 2, pp. 1–5, 2015.

[41] A. J. C. Moreira, R. T. Valadas, and A. M. de Oliveira Duarte, "Characterisation and modelling of artificial light interference in optical wireless communication systems," *Proc. 6th IEEE Int. Symp. Pers. Indoor Mob. Radio Commun.*, vol. 1, pp. 326–331, 1995.

Appendix A

Light Measurements

Table A I - Street Light Illuminance (lux) Measurements

x/y [m]	**0**	**0.5**	**1**	**1.5**	**2**	**2.5**	**3**	**3.5**	**4**
0	19	18.9	18.6	17.9	16.8	15.2	13.7	13.1	11.8
0.5	19	18.9	18.8	18.2	17.2	15.8	14.4	13	12.3
1	19	19.5	19.5	18.5	18.3	16.8	15.4	14.2	13.4
1.5	18.5	18.3	18.6	18.3	17.8	16.5	14.8	13.8	13
2	18	18	17.9	17.3	16.8	15.5	14.8	14.4	13
2.5	16.8	16.6	16.1	16.2	15.1	14.1	13.2	12.9	12.7
3	16.8	14.1	14.7	14.1	14.2	13	12.5	12.3	10
3.5	14.5	14.2	13.9	14	13.5	12.4	11.5	11.1	9.8
4	13.4	14.1	13.5	13.4	13.2	11.7	10.7	10	9.3

Market Weighted Low Beam Headlighting Pattern

Table A II - Luminous intensities (cd) of the low beam headlamps. These entries are the left horizontal side angle measurements, part 1.

Left	**45L**	**40L**	**35L**	**30L**	**25L**	**20L**	**15L**	**10L**	**9L**	**8L**	**7L**	**6L**
7U	21	25	26	30	37	49	73	90	98	107	109	116
6.5U	25	28	29	32	38	51	75	97	104	112	118	119
6U	27	31	34	36	39	54	76	103	112	119	124	126
5.5U	28	31	34	39	42	57	79	112	119	127	132	133
5U	27	31	38	42	46	61	88	121	125	135	144	139
4.5U	27	32	42	46	50	63	90	135	144	152	156	155
4U	26	34	43	50	56	67	96	147	159	169	168	174
3.5U	26	35	43	56	59	75	102	158	169	181	185	194
3U	26	35	44	60	69	87	111	180	192	204	203	211
2.5U	26	36	46	64	79	108	127	198	215	225	225	233

2U	25	35	48	71	90	118	146	219	223	234	253	263
1.5U	25	37	51	78	101	141	176	251	255	272	288	301
1U	25	38	50	80	115	178	208	288	297	318	336	362
0.5U	23	36	54	84	143	226	276	414	415	421	426	446
0	23	38	55	101	177	323	417	673	715	775	829	939
0.5D	22	36	59	122	227	467	694	1307	1474	1699	2022	2338
1D	22	36	62	153	303	700	1090	3062	3285	3455	3946	4747
1.5D	23	35	67	170	384	934	1525	3357	3677	4248	4850	5774
2D	24	34	68	208	521	1368	2310	4438	4781	5089	6034	6835
2.5D	23	33	72	213	596	1749	3004	4614	4909	5315	5809	6670
3D	23	32	72	254	695	1771	3075	5080	5262	5599	6035	6444
3.5D	23	32	71	258	775	1794	2585	4652	5100	5275	5622	5256
4D	24	32	72	257	795	1612	2454	4004	4324	4568	4516	4390
4.5D	23	30	68	239	791	1575	2314	3220	3377	3677	3641	3579
5D	23	31	60	205	685	1334	1905	2476	2679	2895	2909	2941

Table A III - Luminous intensities (cd) of the low beam headlamps. These entries are the left horizontal side angle measurements, part 2.

Left	**5L**	**4.5L**	**4L**	**3.5L**	**3L**	**2.5L**	**2L**	**1.5L**	**1L**	**0.5L**	**0**
7U	111	108	103	100	101	102	104	107	115	124	123
6.5U	114	112	110	111	112	114	117	122	126	137	136
6U	119	118	116	115	120	126	131	137	143	152	148
5.5U	139	131	131	134	142	150	159	163	159	158	169
5U	140	155	154	159	168	180	185	188	183	178	182
4.5U	159	163	176	181	187	203	210	211	208	203	199
4U	176	180	188	197	208	195	200	201	203	208	211
3.5U	200	202	204	215	217	223	229	230	233	239	250
3U	215	221	228	233	237	246	254	257	262	266	269
2.5U	242	250	257	256	261	269	270	274	291	296	317
2U	276	286	298	295	297	305	332	333	348	360	376
1.5U	330	335	351	356	365	372	370	392	425	453	446
1U	390	412	426	443	467	507	500	532	567	607	619
0.5U	496	561	597	647	708	774	835	932	1087	1633	2159
0	1093	1221	1213	1315	1486	1672	2080	2796	4352	6272	8830
0.5D	2691	2921	3491	3663	4022	4541	5366	6760	8750	11788	14555
1D	5306	5904	6338	6573	6960	7130	8823	10570	12513	15840	18902
1.5D	6926	7601	8102	8274	8301	8813	11410	13309	14406	15957	17099
2D	7404	7875	7865	8268	9082	10333	11921	12191	13083	14222	14705
2.5D	7101	7096	7430	8229	8957	8845	9678	10064	10458	11126	11790
3D	6481	6551	7016	7382	7597	7765	7899	8403	8624	8762	8905
3.5D	5449	5702	5842	6015	5949	5932	6472	6580	6505	6572	6773
4D	4448	4581	4730	4855	4855	4955	4964	5017	4993	5052	5157
4.5D	3637	3669	3729	3873	3951	4006	3999	3937	3950	3961	3939
5D	2963	2976	3002	3010	3031	3007	3035	3024	2991	2992	2965

Table A IV - Luminous intensities (cd) of the low beam headlamps. These entries are the right horizontal side angle measurements, part 1.

Right	0.5R	1R	1.5R	2R	2.5R	3R	3.5R	4R	4.5R
7U	117	112	109	109	110	111	119	121	125
6.5U	132	128	131	130	127	130	135	137	138
6U	145	148	151	153	154	155	153	149	147
5.5U	169	174	176	175	173	181	187	192	185
5U	178	177	173	177	186	195	199	203	196
4.5U	200	198	198	198	207	196	214	215	202
4U	217	218	215	216	215	214	219	228	215
3.5U	253	244	236	234	233	234	236	240	246
3U	276	277	276	272	262	259	264	261	246
2.5U	329	330	314	300	296	295	298	291	274
2U	389	395	395	389	380	369	367	365	362
1.5U	452	448	419	432	435	440	440	424	479
1U	589	662	620	578	577	551	600	560	547
0.5U	2393	2391	2387	2578	2815	2520	2206	1684	1415
0	10124	11952	11972	12662	11838	10688	9678	7168	6261
0.5D	18927	18885	18564	17318	16958	15969	14287	12020	9411
1D	21929	22740	21595	20174	19033	16962	14921	13178	11174
1.5D	19076	20241	19534	18785	18074	17209	16324	13592	11002
2D	16457	16273	16247	15821	15442	15130	14545	13626	11242
2.5D	12335	12550	12603	12605	12491	12265	11860	11221	10115
3D	9088	9294	9281	9208	9265	9314	9221	9025	8511
3.5D	6660	6719	6748	6943	7303	7251	6920	6686	6471
4D	4990	5025	5137	5152	5347	5237	5072	4964	4830
4.5D	3962	3936	3911	3884	4107	4085	3899	3792	3658
5D	2960	2930	2953	2973	3027	2993	2970	2929	2845

Table A V - Luminous intensities (cd) of the low beam headlamps. These entries are the right horizontal side angle measurements, part 2.

Right	5R	6R	7R	8R	9R	10R	15R	20R	25R	30R	35R	40R	45R
7U	120	116	108	93	88	85	60	42	30	17	10	8	5
6.5U	138	134	129	101	94	91	66	47	33	18	10	8	5
6U	146	145	121	115	103	97	65	49	33	18	11	7	4
5.5U	169	149	157	122	114	105	69	50	35	20	11	7	4
5U	173	159	152	131	122	108	77	59	38	21	11	8	5
4.5U	192	165	162	143	136	115	86	65	39	21	12	8	5
4U	222	181	174	153	145	126	92	72	45	21	12	8	5
3.5U	223	215	191	182	172	152	102	78	50	23	13	8	5
3U	225	213	204	200	185	159	113	88	53	25	14	8	5
2.5U	276	271	264	231	207	185	129	97	63	27	16	7	4
2U	345	303	294	263	237	219	146	110	71	33	15	8	5
1.5U	423	370	342	332	294	282	188	127	75	38	14	8	4

1U	576	511	451	426	373	354	241	171	79	44	13	7	4
0.5U	1201	875	694	582	560	519	340	224	97	52	13	7	4
0	4717	3092	2319	1540	1200	1120	514	333	107	55	13	6	4
0.5D	7896	5457	3918	3290	2632	2275	859	486	111	53	12	7	4
1D	9898	7295	5378	4221	3551	2801	1401	691	140	50	15	7	4
1.5D	10257	8096	6429	5195	4632	4237	1968	867	191	50	14	6	4
2D	10498	8180	7105	5902	5122	4399	2516	1089	235	51	12	7	4
2.5D	9231	7600	6701	5599	5155	4932	3108	1103	290	50	13	6	4
3D	7795	6936	6186	5788	5457	4958	2969	1184	319	50	17	6	5
3.5D	6309	5957	5399	5084	4782	4342	2638	1280	337	48	15	7	4
4D	4708	4513	4306	4138	3880	3785	2301	1276	355	49	13	7	4
4.5D	3552	3564	3490	3287	3111	2978	2170	1216	368	50	12	7	4
5D	2813	2819	2662	2625	2582	2367	1721	1097	319	57	13	6	4